AN ABSTRACT OF THE THESIS OF

Michelle L. Murillo for the degree of Master of Science in Forest Science presented on December 7, 2000.

Title: Modeling Slope Stability Uncertainty: A Case Study at the Andrews Experimental Forest.

Abstract approved: _____

Frederick J. Swanson

A simple debris-slide model, employing a digital elevation model (DEM) and geological data, was used in a geographic information system (GIS) to map slope stability in the Andrews Experimental Forest, located in the western Cascade Range in Oregon, USA. To evaluate the contribution of error in elevation to the uncertainty of the model output, several different, but equally probable, perturbed versions of the input DEM were created by adding random, spatially autocorrelated error files. These perturbed DEMs were then processed to produce a family of slope-stability maps from which the effects of elevation error upon debris-slide potential could be assessed. The DEM error had a significant effect on the DEM-derived slopes and subsequent classification of debris-slide potential. These effects were attributed to the manner in which the debris-slide model is derived and the slope algorithm used in the GIS. The maximum magnitude of elevation error (+/- 7m) added to the DEM was small relative to variation in the height of tree canopies (0-70m) across the landscape (which can influence resolution of photogrammatrically-based interpretations of topography). The ability to assess this uncertainty has the potential to to increase understanding of inherent

strengths and weaknesses of applying digital data and spatial information systems to this application, and to facilitate improved natural resource management decisions in relation to timber harvesting and slope stability problems.

Modeling Slope Stability Uncertainty: A Case Study at the Andrews Experimental Forest

by

Michelle L. Murillo

A THESIS

submitted to

Oregon State University

in partial fulfillment of
the requirements for the
degree of

Master of Science

Completed December 7, 2000
Commencement June 2001

Master of Science thesis of Michelle L. Murillo presented on December 7, 2000

APPROVED:

Major Professor, representing Forest Science

Chair of the Department of Forest Science

Dean of the Graduate School

I understand that my thesis will become part of the permanent collection of Oregon State University libraries. My signature below authorizes release of my thesis to any reader upon request.

Michelle L. Murillo, Author

Approved by Committee:

Major Professor (Frederick J. Swanson)

Committee Member (Bose)

Committee Member (Curtis R. Cook)

Committee Member (Paul Cull)

Graduate School Representative (Rod A. Harter)

Date thesis presented December 7, 2000

ACKNOWLEDGMENTS

This study would not have been possible without the support of the National Science Foundation's Andrews Forest Long-Term Ecological Research (LTER) site and the USDA Forest Service, Pacific Northwest (PNW) Research Station, Corvallis, Oregon. Data sets were provided by the Forest Science Data Bank, a partnership between the Department of Forest Science, Oregon State University (OSU), and the PNW Research Station. Funding for these data was provided by the LTER program and other National Science Foundation programs (NSF), OSU, and the PNW Research Station.

I am gratefully indebted to Dr. Frederick Swanson for believing in the importance of this study and for never giving up on the possibility we might actually get it done. I would like to especially thank Dr. Phil Sollins for coming on board at the end and jumping in head first without much persuasion. Additional editorial assistance and support were provided by my other committee members; Drs. Jon Kimerling and Paul Doescher. A very special thanks to Dr. Gary Hunter, Associate Professor and Reader, Department of Geomatics, University of Melbourne, Australia. Dr. Hunter provided invaluable assistance with his Uncertainty Model and provided assistance and guidance in the initial development and planning of this project.

Many others also merit recognition for their assistance in conducting this research and in preparation of this paper. George Lienkaemper of the United States Geological Survey provided countless answers to my GIS questions and issues, and always with a smile! Mark Gray, Michael Murillo, and Randy Roberts of Los Alamos National Laboratory (LANL) acted as resident "advisors" by providing insight and discussion into the details of the results, offering overall suggestions

and guidance, and helping fix several of the major glitches along the way. Tom Evans and Chris Fontes of LANL provided assistance in the formatting of the thesis.

Completing this project required copious amounts of persistence on my part, as well as that of others. I would like to thank my family and friends who provided unending support, confidence, and encouragement in completing this project. Thanks to Ken West for assisting with the presentation and the final stages. Thanks to Robin Reynolds, Terri Morris, and Barbara Maydew for always being there and providing the extra confidence boost when needed. A very special thanks to Sheila Wasfey who tenaciously provided a ticking clock until the very end by rigidly scheduling mock defenses (with pizza and sushi), and then by assimilating the difficult questions and suggestions posed by the resident "advisors".

TABLE OF CONTENTS

TABLE OF CONTENTS (Continued)

LIST OF FIGURES

LIST OF FIGURES (Continued)

LIST OF TABLES

LIST OF TABLES (Continued)

DEDICATION

This study is dedicated to my brother Michael without whom most of the wonderful things in my life would not be possible and to my grandfather Charlie for teaching me how to fish.

MODELING SLOPE STABILITY UNCERTAINTY: A CASE STUDY AT THE ANDREWS EXPERIMENTAL FOREST, OREGON

1. INTRODUCTION

1.1. Background

The Pacific Northwest of the United States contains some of the most productive temperate forests in the world and timber harvesting has been a primary land use in the area for over 100 years. Much forest land in the region is in mountainous terrain with areas of weak rock and soil and steep slopes prone to various types of debris slide processes. Land use activities can decrease slope stability and therefore may increase rates of mass movements [1], [2], and [3]. One of the major concerns associated with debris slides is the cumulative effect it has on the entire watershed, such as decreased water quality, loss of spawning habitat, and debris jams that may break during peak river flows, thereby scouring channels and disturbing riparian vegetation. Thus, the ability to predict location of slope failure and understand basic controls on the process is useful in evaluating impacts of forestry practices and minimizing undesirable effects [4].

While methods such as ground and aerial surveys can aid in locating existing and potential debris slide areas, they also suffer several disadvantages. For example, in the western Cascade Range, ground surveys are difficult to conduct since accessibility is a major problem in a region characterized by steep slopes, few roads, and thick vegetation cover [4]. This effectively reduces the extent of terrain that can be covered, which in turn may lead to an underestimation of debris slide occurrences and misinterpretation of management effects.

Similarly, there can be difficulties in obtaining and interpreting suitable aerial photography as a result of highly variable weather and climate conditions. Seasonal considerations consequently limit accurate photographic interpretation. Debris slides tend to occur during the winter rainy season during major storms. This would be the optimal time to conduct a debris slide inventory. Unfortunately, this is when cloud cover is most prevalent and access is most limited. Also, some debris slides may be too small to be detected by aerial photography [5]; too difficult to identify because they are either hidden under the dense forest canopy [6], masked in shadow by steep, narrow ridges and tall, dense vegetation [7].

Another approach to examining debris slide patterns is to use a Geographic Information System (GIS) to model debris slide hazard potential by considering the critical topographic factors that influence spatial patterns of slope stability. Field and theoretical studies indicate that slope steepness, soil and vegetation are major determinants of slope stability. GIS techniques permit large-scale evaluation of influences of topographic and other factors on geographic patterns of slope stability. These techniques commonly lack consideration of the uncertainty of the final output resulting from errors occurring in the topographic parameters used to model potential slope failure. GIS fosters an environment in which data transformations can be performed quickly without the need to understand how the result is achieved. These operations use spatial relations implicit in the source data and, in the process, transform the existing uncertainty and subsequently propagate this uncertainty through the operations performed on the source data [8], [9]. In order to maintain an assessment of the data quality in a GIS-based analysis, the propagation of this uncertainty must be accounted for throughout the entire process. This provides a dependable data quality analysis from the source to the final output of the GIS analysis.

Ideally, formal mathematical models would be applied to illustrate and state explicitly how particular data transformations alter error in source data, the modeling process, and the final output. This approach requires established error models for spatial data handling processes and knowledge of error propagation behavior when using spatial databases. Only a limited number of error models are available and generally do not provide sufficient detail to describe the complexity of the error and error propagation inherent in the GIS transformation of spatial data [9]. Consequently, obtaining an actual assessment of uncertainty and its propagation through GIS analysis is not trivial and is not part of the focus of this thesis.

As an alternative, Hunter and Goodchild [10] developed an experimental uncertainty assessment technique employing a stochastic mechanism to generate a series of perturbed input values for spatial models. These values were then used in a GIS analysis to produce a visual representation indicating the functional relationship between the final output and the source data and subsequent data transformations. This approach provided a first approximation of the effects of uncertainty in the DEM and is easily accomplished. Moreover, it has wide applications in many fields of spatial data handling, such as land suitability/capability analysis, soil classification, viewshed calculations, and hydrologic modeling in general.

This study applies the uncertainty model developed by Hunter and Goodchild [10], [11] to examine the uncertainty in a slope stability model by utilizing digital elevation models (DEM) for the Andrews Experimental Forest in the western Cascades of Oregon. The debris-slide model combines slope gradient values with a generalized geology map to yield debris slide hazard classes. Different, but equally probable, versions of source DEMs were created through the creation of

random, spatially-autocorrelated elevation noise files. The DEMs were then processed to produce a family of slope class maps for which the effects of error in the DEM upon the final debris slide model indices could be assessed. Using this alternative model, formal mathematical error analysis is bypassed, yet a simple but effective visualization and qualification of the uncertainty is achieved.

This study applies the uncertainty model developed by Hunter and Goodchild [10], [11] to examine the uncertainty in a slope stability model by utilizing digital elevation models (DEM) for the Andrews Experimental Forest in the western Cascades of Oregon. The debris-slide model combines a slope gradient map with a geology map to yield a debris-slide hazard map and is a common manner in which a GIS is used to produce a new map. However, this approach commonly contains no consideration of the uncertainty associated with the final stability map. Application of the uncertainty model to assess the cumulative effect upon the final debris-slide hazard rating derived for each cell is used, given that the slide hazard map is a function of: 1) the DEM resolution and its estimated elevation error, 2) the slope gradient calculation for each cell, and 3) the method of classifying the slopes and rock types to derive the index. Using this alternative model, formal mathematical error analysis is bypassed, yet a simple but effective visualization and qualification of the uncertainty is achieved.

1.2. Characteristics of Andrews Experimental Forest

The Andrews Experimental Forest is used as a site for examining effects of error in spatial databases used in watershed studies. The Andrews Forest is located approximately 80km east of Eugene, Oregon. The Lookout Creek basin, the test area, comprises the forest and drains nearly 6400 hectares in the western Cascade

Range. The overall site was established as an Experimental Forest in 1948 after which trial forest harvests, concomitant road construction, and various watershed and ecological studies occurred throughout the 1950's and 1960's. Since 1970, site emphasis has shifted to ecosystem research and the levels of timber harvesting and road building have been reduced.

The Andrews Forest geologic history contains discrete stages of volcanism interspersed with periods dominated by weathering, erosion, and the reworking of volcanic material [12]. Since the late Pliocene alluvial, glacial, and mass movement processes have shaped the present Lookout Creek basin. The upper areas of Lookout Creek Basin are formed from lava flows ranging in age from 3 to 13 million years, while lower areas are underlain by older (14 to 25 million years BP), more weathered and hydrothermally altered clastic volcanic rocks.

Two types of landslides occur in the basin. The most common are relatively small (averaging approximately 2000 cubic meters), shallow, rapid debris slides comprised mainly of soil, colluvial, vegetative material that take place on hillslopes during intense rainfall and rain-on-snow events [12]. The second type is relatively large, deep-seated, slow-moving earthflows that move seasonally at rates varying from centimeters to meters per year. Earthflows tend to occur in volcaniclastic rock terrains where lava flow rocks cap clastics [12]. This instability occurs in part, because overlying lava flows have open fractures and joints that permit rapid movement of water into the contact zone and into the marginally stable rock below the contact zone. During heavy rain storms the rapid influx of water creates high pore water pressures, increasing the probability of a mass movement of both types.

Extensive inventories have been conducted which documented over 140 debris slides since 1950 in the basin [13], [14], [4]. The mapping of mass movements conducted by Swanson and James [12], Swanson and Dyrness [14], and Dyrness

[13] has demonstrated that the bedrock geology and slope steepness exercise a significant influence on the occurrence of deep and shallow mass movements in this area of the Western Cascades.

2. LITERATURE REVIEW

2.1. GIS Error History

Traditionally, cartographers compensate for errors and uncertainty with the use of experience and expert knowledge to prepare maps and analyze map-based data. For example, consider the case in which a stream appears on a map to flow upwards based on the configuration of the contour lines. The cartographer would adjust the contour lines or move the stream to compensate for this error. The advent of digital processing of spatial data with a GIS has led to the automation of map preparation, including combining multiple data sources in a transparent and automated manner and using multiple scales, projections, and data models. While this approach is significantly faster than traditional methods, a considerable amount of cartographer experience in error detection and elimination is lost. Citing the previous example, the capability of a GIS to manipulate the stream/contour line relationship is limited to a special case implementation of a specific algorithm; i.e. one cannot describe in general terms an algorithm that will enforce accuracy in the GIS transformation process. Furthermore, GIS data output has a high level of numerical precision (determined by the machine floating point arithmetic) which provides the illusion of accuracy. This accuracy is generally not warranted; for example, the location of a feature on a printed map may only be accurate to three significant figures, but a computer can store and calculate many more figures [15].

Several authors have described GIS processing errors in detail ([16], [17], [18], [19], and [20]). In general GIS errors are found in 1) source data, 2) data transformation, 3) data processing, and consequently in 4) the data output. Source data errors are of the type that arise from mistakes made taking the measurements, from faulty recording or measuring equipment, or from the inherent properties of

nature (fuzzy data). Data transformation errors arise when data are transformed from a non-GIS source, (such as a paper map or a satellite image) into a GIS format. Data processing errors range from blatant errors such as overlaying two maps with different coordinates to inappropriate phrasing of spatial queries (i.e. data are not suited for the question). Some other sources of data processing error in GIS processing include the generalization (or aggregation) and de-generalization (or disaggregation) of data, and similarly classifying and reclassifying data. Lastly, with this potential for error at each step of GIS processing, it is not surprising that the data output will contain some amount of error that has been propagated through the process.

While a reasonable understanding of most of the source errors listed above exists, research is lacking for the theory and modeling of error propagation that considers the interaction of spatial database accuracy, formal methods of error propagation [21] and methods using standardized techniques to quantify and report error [22], [21]. Error propagation modeling applies mathematical techniques to describe the manner in which source error is modified by GIS transformation functions [21]. Error propagation is not well understood for most GIS transformations; little is known about the theory of GIS error propagation and models that describe propagation are not generally available. The use of a rigid mathematical description to describe the mechanism of the modification of source error in the data transformation process is one approach to modeling error propagation. This mathematical approach may be based on statistical theory, probability theory, or series expansions [21]. Unfortunately, the formal technique is unwieldy as little is known about the theory of error propagation, and models describing propagation remain to be developed.

Alternatives exist to the formal approach. One popular methodology is to use a Monte Carlo technique [21]. This scheme is based on the random introduction of error to create a set of scenarios that represents the nature and magnitude of error present. This result is subsequently passed through the transformation functions in an iterative manner to calculate an error summary based on assumptions about the nature of the error in the products of the transformations. Similarly, another study simulated the effect of input data error by introducing random 'error' to the line co-ordinates in map data [18]. This random 'error' simulates the combined source map and map processing errors by slightly altering the shape of the line. This process is repeated until a statistically sound number of results has been produced, and these results are then compared with the normal, unvaried maps.

Another approach to the modeling of errors in spatial data is the 'Perkal epsilon band method' developed by Perkal and subsequently modified by Chrisman [23](Figure 2.1).

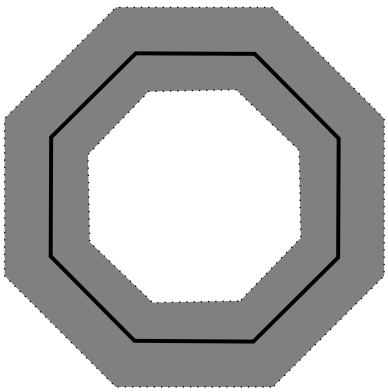

FIGURE 2.1. Depiction of the Perkal epsilon method.

This technique is based on the concept that the true position of a line can be described as some displacement from the measured position. This concept es-

sentially defines a mean probable location of the line within a probability density function, resulting in a technique for the measurement of errors in area. Several authors ([15], [24]) dispute the usefulness of this model in describing errors as it does not provide a stochastic process to model error. For example, the observed position of an edge of a polygon may lie inside or outside the true position; the integral of this curve over the polygon would result in these edge effects essentially canceling each other in an area calculation, overestimating the true uncertainty. Goodchild suggests the use of distorted lines or polygons as a basis for the comprehensive analysis of error and it provides a stochastic process of modeling the error (Figure 2.2).

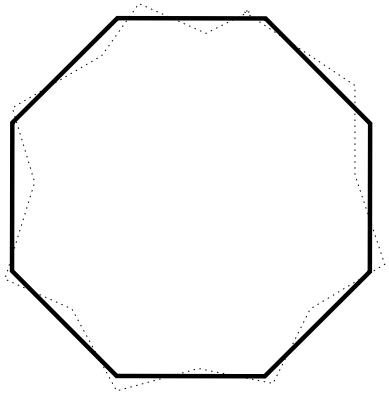

FIGURE 2.2. Depiction of of alternate Perkal epsilon method.

In this thesis presentation, yet another alternative model, the Uncertainty Model [10], is presented as a relatively easy to use tool that can give users an understanding of how sensitive their data may be to uncertainty and its subsequent propagation.

2.2. The Uncertainty Model

Before discussing the uncertainty model used in this research, some explanatory remarks are required regarding the term 'uncertainty'. In general terms, it denotes a lack of sureness or definite knowledge about an outcome or result. In the context of GIS, it has been suggested that there is a clear distinction between 'error' and 'uncertainty,' since the former implies that some degree of knowledge has been attained about differences between actual results or observations and the truth to which they pertain. On the other hand, 'uncertainty' conveys the notion that it is the lack of such knowledge that is responsible for our hesitancy in accepting those same results or observations without caution. The term 'error' is often used when it would be more appropriate to use 'uncertainty.'

The uncertainty model used here is a version of the one originally developed by Goodchild et. al. [9]. In general it may be defined as a stochastic (random) process capable of generating a population of distorted versions of the same spatial data set, with each version being a sample from the same population. The traditional Gaussian model (where the mean of the population is an estimate of the true value and the standard deviation is a measure of the variation in observations) is one attempt at describing error, but it says nothing about local variation or the processes by which it has accumulated. The model applied here is viewed as an advance over the simple Gaussian approach because spatial variation in uncertainty can be shown. The model also has the capacity to include in its simulations the probable effects of error propagation resulting from the various algorithms and processes that have been progressively applied to the data sets employed. By studying different versions of the final output, it is possible to see how differences in input

affect the outcome, and in essence the purpose of the model could be described as an attempt to "find a Gaussian distribution for maps" [9].

It has been argued by Hunter and Goodchild [11], that while it is possible to distort a data set according to an error description (e.g. the root mean square error (RMSE)) without any consideration of the likely spatial autocorrelation between sample elevations, the process may be stochastic but inevitably lacks a certain 'truthfulness'. In this case, adjacent elevations in DEM which are otherwise similar in value can be severely distorted, thereby creating large topographic pits and peaks which often may not occur in nature. This type of distortion approach produces what are known as 'random maps.'

On the other hand, the assumption of complete spatial dependence between neighboring points produces simulations of a DEM which appear 'truthful' but not stochastic. Elevations are unnaturally constrained to maintain their relative differences to each other and the introduction of a noise component has the effect of shifting all DEM elevations up or down by a constant amount. Hence, there is a need to find a value in the domain $0 < \rho > 0.25$ (where ρ is a measure of spatial autocorrelation) which meets the requirement of being both stochastic and 'truthful.' The limit of 0.25 ensures stationarity (as discussed in Cliff and Ord [25] when the Rook's case (cells that a chess 'rook' could move to) is used to test a cell's elevation against its four neighbors sharing a common edge.

2.3. Errors in Digital Elevation Models

As the main error source in the debris-slide hazard model is the USGS DEM, this section describes the DEM and the errors that are associated with it. The United States Geological Survey (USGS) is the primary producer of extensive

DEMs in the United States. DEMs are constructed by digitizing contours on existing maps or by scanning stereomodels of aerial photographs. Data in a DEM are supplied as a grid of point elevations typically as a 7.5 minute quadrangle map with a 30-meter horizontal ground resolution. These models can then be used to derive a variety of variables, including slope, aspect, slope orientation (combination of slope and aspect), viewshed calculations, and mean, maximum, and minimum altitude.

The USGS classifies DEM errors into three categories; blunders, systematic, and random [26]. Blunders are gross errors that are usually detected and corrected before the DEMs are released. Systematic errors are non-random errors that evolve from procedures that introduce biases and artifacts into the DEM, such as vertical elevation shifts, misinterpretation of terrain surface due to trees, buildings and shadows, and fictitious ridges, tops, benches or striations. One example is striping that occurs when elevation values along one axis are re-sampled at a higher spatial resolution than was used to initially collect the elevation values [26], Theobald 1989). It has been estimated that about 1/3 of the 30m DEMs show this striping (Elassal and Caruso 1983). The third type of error, termed random, results from measurement error that reduces precision (exactness), but does not introduce bias (systematic error). The USGS tests DEM accuracy by comparing elevation values of the DEM with no less than twenty points of known elevation. These discrepancies are usually mapped to a single index representing horizontal accuracy, root mean square error (RMSE). This global representation of the error does not provide any information about where the error may be occurring. The RMSE is then calculated and used to classify DEMs into three qualitative levels, I, II, and III [26], [27] .

Level I DEMs contain no elevation points with an error of more than 50 m and are considered to be the lowest quality. Level II DEMs have no points where the elevation is in error by more than twice the contour interval and the maximum RMSE is 7m. Level III DEMs are more accurate and are similar to Level II DEMs and the RMSE of one-third of the contour interval not exceeding 7m is the maximum allowed. However, these RMSE values are applied globally to the entire DEM and thus, provide no information on how accuracy varies across the DEM.

2.4. Summary

A GIS can perform automated map preparation and analysis used for the combination of various spatial data sources. Unfortunately, when uncertainty exists in the source data, these uncertainties are propagated through the GIS transformation process and degrade the accuracy of the final output. Digital elevation models are often used in many GIS-based natural resource assessments, and are known to contain varying amounts of error. Furthermore, other variables, such as slope and aspect, derived from a DEM are susceptible to uncertainty depending on the terrain. Error modeling can be used to assess the accuracy of the final output of a GIS analysis. Few error models consider the transformation and propagation of error within the GIS analysis. Models describing specific GIS transformation functions (e.g. buffer and overlay) have been developed. However, the understanding of many more GIS operations remain to be explored. Alternatives have been developed, such as the Monte Carlo technique and the uncertainty model.

3. DATA SOURCES

3.1. Field Data

Debris-slide hazard data were collected in the field by various individuals at the Andrews Forest and stored in a database provided by the Forest Science Data Bank, a partnership between the Department of Forest Science, Oregon State University, and the U.S. Forest Service Pacific Northwest Research Station, Corvallis, Oregon. It contains information such as debris-slide initiation site (hollow, hillslope, or streamside slide, or streamside earthflow), elevation, and the slope at each of the debris slides. Table 3.1 provides summary information about the landslide initiation site type.

	Total Number
Hillslope slides	48
Hollow slides	29
Streamside earthflows	22
Streamside slides	23
Points	121

TABLE 3.1. Summary information for field collected slide hazard data.

3.2. USGS Digital Elevation Model

To produce a DEM for the Andrews Forest, several Level II DEMs (30m x 30m cell resolution; 7m RMSE) produced by the United States Geological Survey

(USGS) were used. (The study site DEM was clipped from the following merged DEM's: Carpenter Mountain, Tamolitch Falls, Blue River, McKenzie Bridge, Belknap Springs, and Tidbits Mountain). The Andrews Forest occupies some 70,026 cells or 53 percent of this merged DEM (Figure 3.1). Elevations in the basin range from 411 meters above sea level in the southwest to 1615 meters in the northeast.

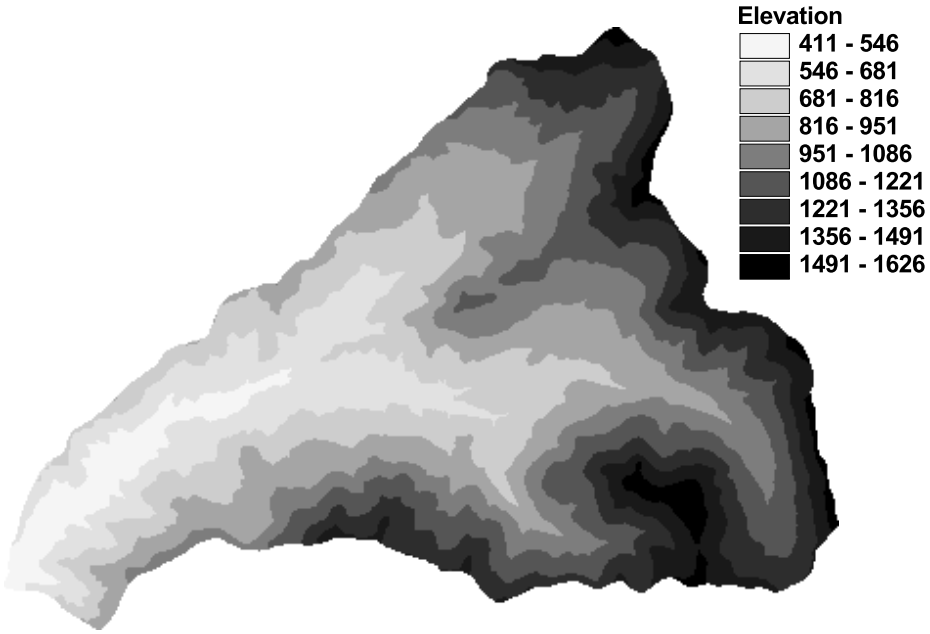

FIGURE 3.1. DEM of the Andrews Experimental Forest.

3.3. Debris-Slide Hazard Map

To produce the debris-slide hazard map, two maps in grid form are required. The first is a map displaying geologic information at the same grid cell size and georeferencing as the DEM. In this geology map, bedrock was classified by strength, with young lava flows and intrusive bodies being graded as strong; intermediate-age, clastic rocks, including well-welded ashflow units, as moderate strength; and

old, hydrothermally altered clastic rocks (18-25 millions BP) as weak (Figure 3.2). The second map is a slope class map which is derived from the DEM. (see section 4.2).

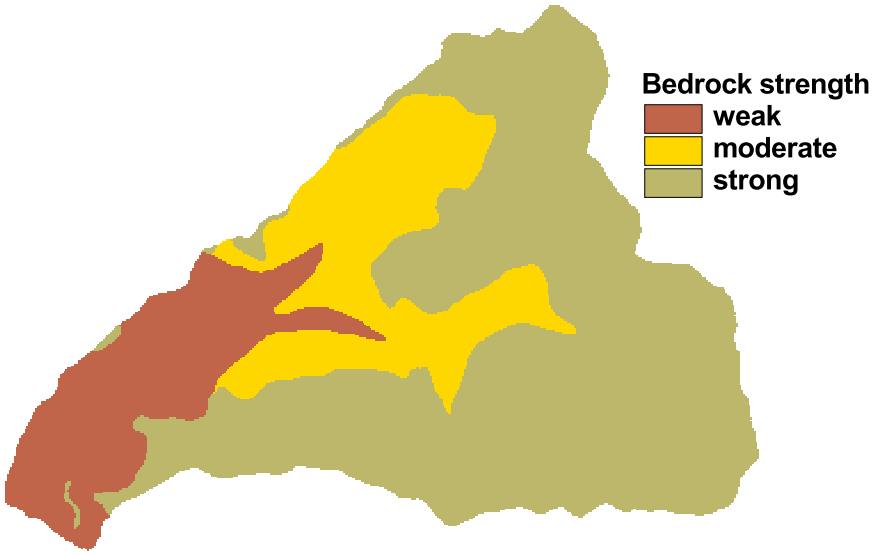

FIGURE 3.2. Bedrock strength classes of the Andrews Experimental Forest.

3.4. Debris-Slide Location Map

The location of the debris slides found in the field (see section 3.1) were digitized into the ARC/INFO POINT map LSPOINTS (provided by the Department of Forest Science). This map allows one to determine attributes of a particular point where a debris slide occurred. Figure 3.3 shows the original debris-slide hazard map with the location of the debris slides measured in the field. Additionally, the type of land use area attribute was added into the LSPOINTS map for each debris slide location. Table 3.2 provides summary information about the land use type in the LSPOINTS map.

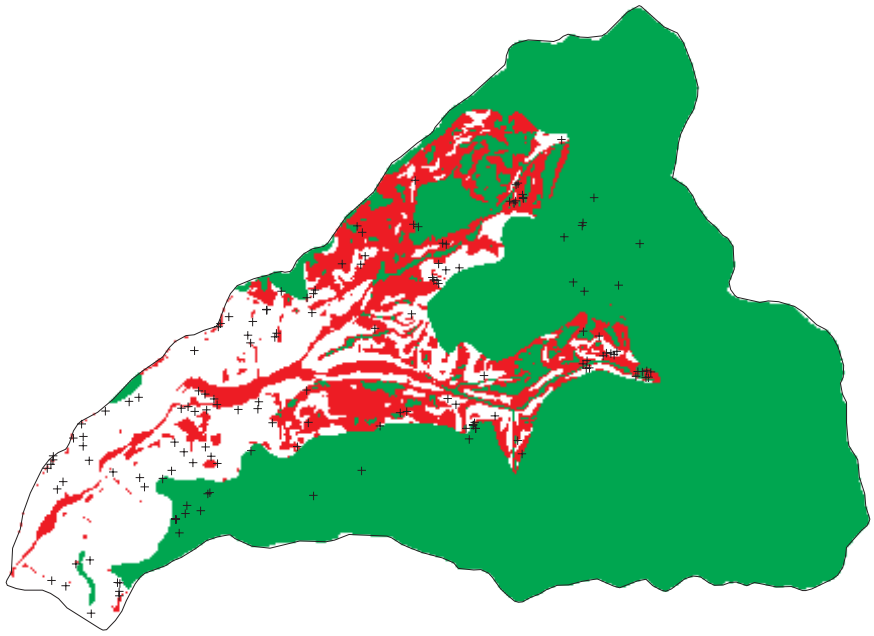

FIGURE 3.3. Original slide hazard map with inventoried slides shown as a '+'.

	Total Number	**Area (approx. ha)**
Forest	56	4418
Clearcut	65	1310
Road	25	236
Points	145	6000

TABLE 3.2. Summary information for debris slide inventory data.

4. PROCEDURES

4.1. Debris-Slide Attributes

Using the ARC/INFO Grid module function CELLVALUE, attributes such as slope, slopeclass, landuse type, and debris-slide hazard rating can be determined at each of the 145 debris-slide sites that were measured in the field (see section 3). These data are stored into the LSPOINTS map. The function CELLVALUE returns the value of the attribute in the center of the cell. Slope and slope class refers to the slope from the DEM and not from the field data.

The attributes can then be downloaded into an ascii text file using the UNLOAD function in the ARC/INFO module TABLES. These data are then used to perform an analysis of the field and original data, and an analysis on the original and perturbed data.

4.2. Debris-Slide Hazard Map

The procedure described here to create the debris-slide hazard map is identical whether you are using the original or the perturbed DEMs. In deriving the debris-slide hazard map, the slope gradient is calculated for each cell in the DEM (using the 4-neighbor SLOPE function within the ARC/INFO Grid module) (Equation 4.1) and then reclassified into 3 categories - greater than 20^o representing steep slopes, 10-20^o for moderate slopes, and $< 10^o$ for gentle slopes to produce a slope class map (Equation 4.2).

$$grid\_slope = slope(DEM) \tag{4.1}$$

$$grid\_slopec = slice(grid\_slope, table, classificationtable) \tag{4.2}$$

Using the ARC/INFO Grid function COMBINE, the geology map and the slope class maps (Figure 4.1) are combined to produce the debris-slide hazard map (Figure 4.3). This map is then reclassified into the three levels of debris-slide hazards - high, moderate, and low (Table 4.1 and Figure 4.2).

$$grid\_hazard = combine(grid\_slope, geology) \tag{4.3}$$

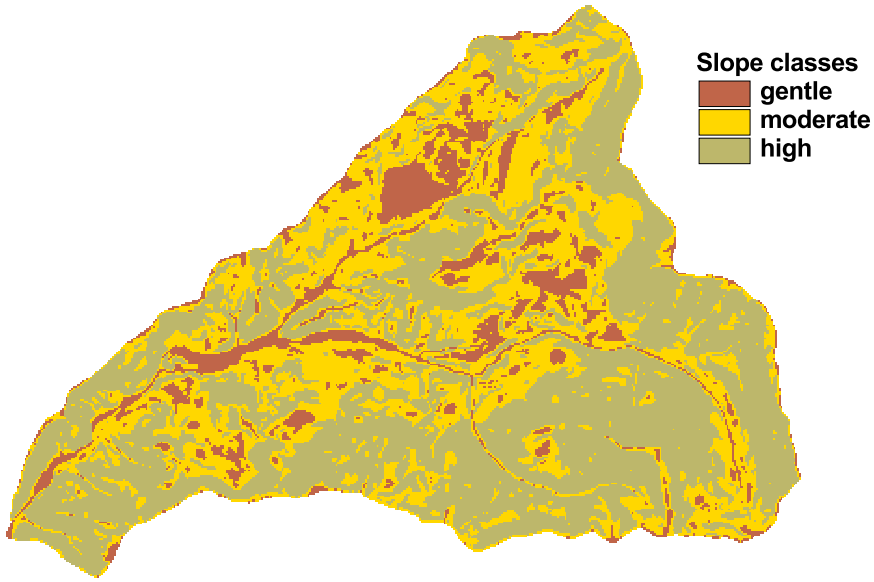

FIGURE 4.1. Slope gradient classes of the Andrews Experimental Forest.

	bedrock strength		
slope	**strong**	**moderate**	**weak**
$0^o < 10^o$	low	low	moderate
$10^o - 20^o$	low	moderate	moderate
$> 20^o$	low	high	high

TABLE 4.1. Derivation table for debris-slide hazard rating.

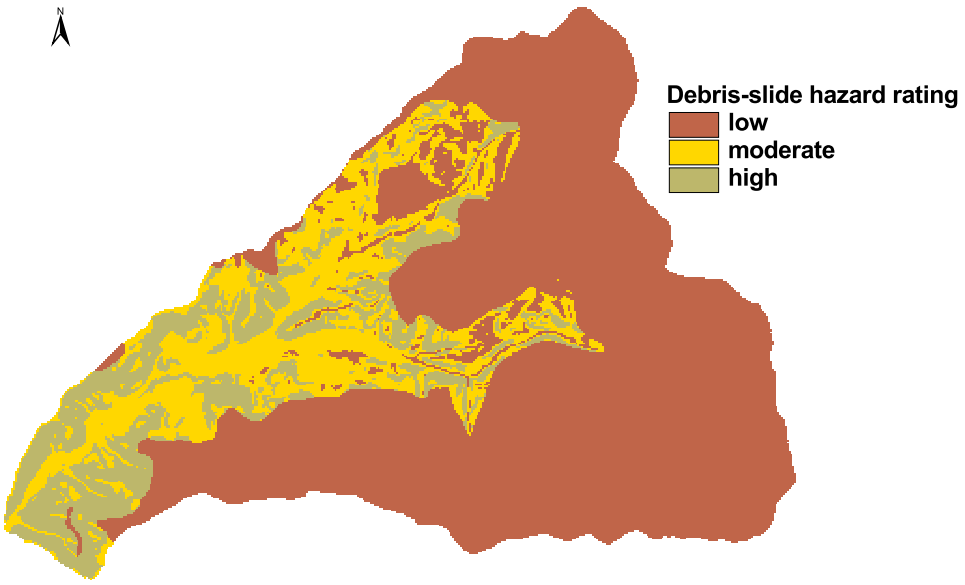

FIGURE 4.2. Debris-slide hazard map of the Andrews Experimental Forest.

4.3. The Uncertainty Model

Application of the uncertainty model consists of four stages (Figure 4.3), with the first stage requiring the user to combine whatever data, processes and models needed to generate the desired output - in other words, applying the GIS as would normally occur without any consideration of uncertainty [28]. In this study, a debris-slide hazard map is generated (see section 4.2).

In the second stage, the parameters necessary to create perturbed DEMs are obtained. This includes the number of rows and columns in the original DEM, the cell size, and geo-referencing details. An error estimate for the original DEM will also need to be identified as this is usually a global value of the elevation error present. In this case the RMSE as supplied by the DEM producer is used. These parameters will be required in stage three of the uncertainty model (Table 4.2).

parameters	**value**
CELL SIZE(m)	30
XMIN UTM COORDINATE(m)	558946.072
YMIN UTM COORDINATE(m)	4893975.967
Number of rows	308
Number of columns	427
DEM RMSE(m)	7

TABLE 4.2. Parameters necessary to create the perturbed DEM.

In stage three of the methodology, ten perturbed DEMs of each initial ρ value are generated using ρ values of 0.0, 0.05, 0.10, 0.15, 0.20, 0.21, 0.22, 0.23, 0.24, 0.245, and 0.249. The first step in producing perturbed DEMs is to create

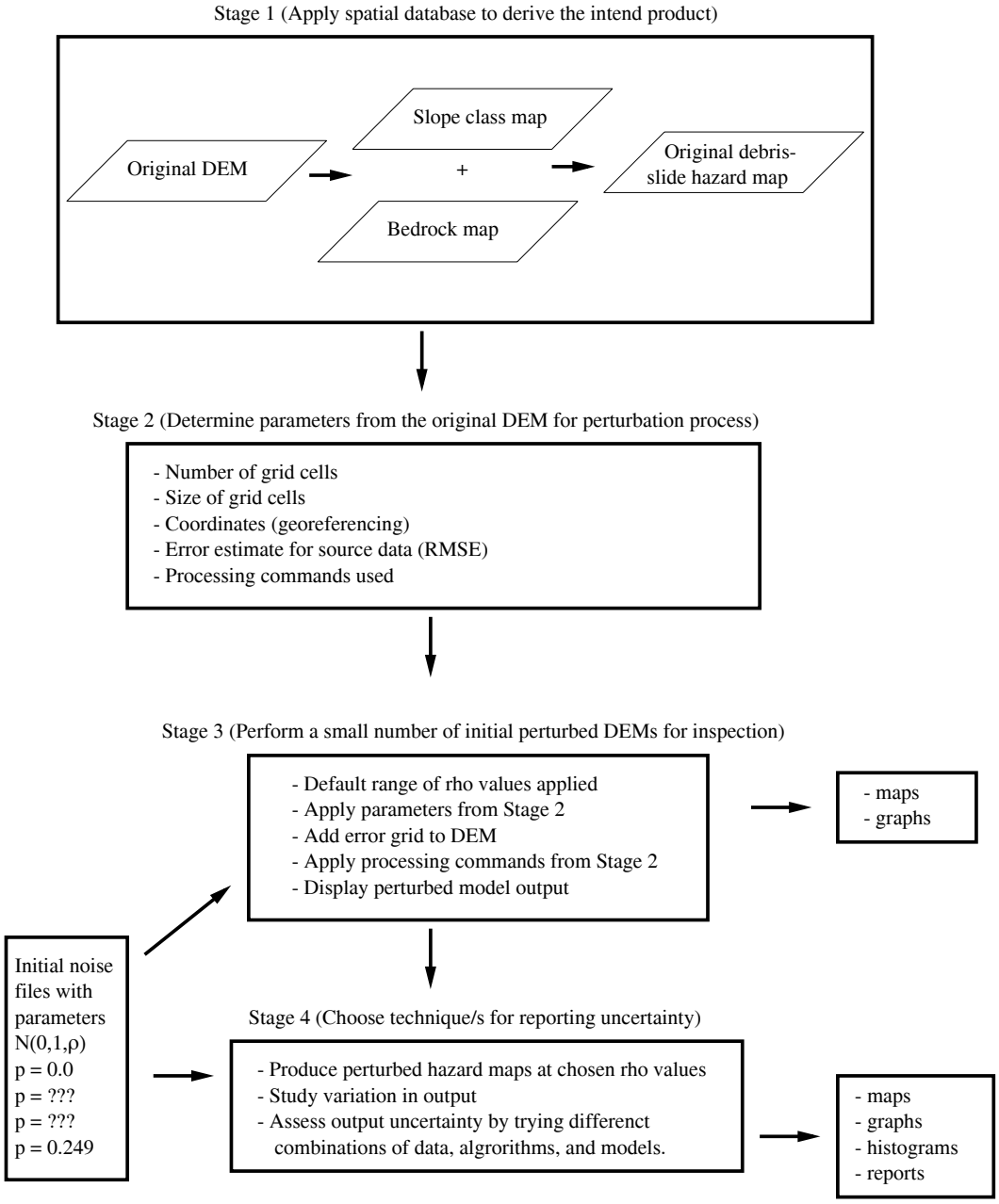

FIGURE 4.3. The four stages of the uncertainty model.

noise grids containing random numbers drawn from a normal distribution with mean zero and standard deviation of 1. Each of these noise grids are reprocessed to take into account the desired ρ value, by systematically computing a new value for each cell to be equal to the sum of the four adjacent cells multiplied by ρ plus the original random value μ, as in equation 4.4 below where $\epsilon_(i,j)$ is the new error component for the cell in row(i) and column(j).

$$\epsilon_{i,j} = \rho(\epsilon_{i,j-1} + \epsilon_{i+1,j} + \epsilon_{i,j-1} + \epsilon_{i,j+1}) + \mu \tag{4.4}$$

To illustrate this process, figures 4.4, 4.5, 4.6, and 4.7 display several of these noise grids. Note that for ρ values up to 0.20 no distinct patterns occur, indicating no major differences in the spatial autocorrelation. Distinct patterns do begin to emerge as the ρ value increases above 0.20, especially as the value approaches 0.25 (the maximum spatial autocorrelation). At ρ values higher than 0.20 clustering is seen in small groups of cells. At $\rho = 0.245$ the clustering effect is strong and the variation in the values between neighboring cells is heavily constrained. In effect, there will no longer be neighboring cells with radically different values and so large transition zones appear surrounding white and black clusters that represent extreme values. In addition, the high ρ values also act as a filter that removes the extreme values from the simulation and only the more general trends remain. Therefore, at high ρ values a very smooth image with no abrupt changes in value would be expected.

In the next step,the noise grid first needs to have the mean and standard deviation adjusted to equal that of the DEM to which it will be added. To do this, the noise grid mean and noise grid standard deviation from each noise grid are obtained using ARC/INFO. These values are used to create a temporary grid which will have a mean of zero (the value usually adopted by data producers

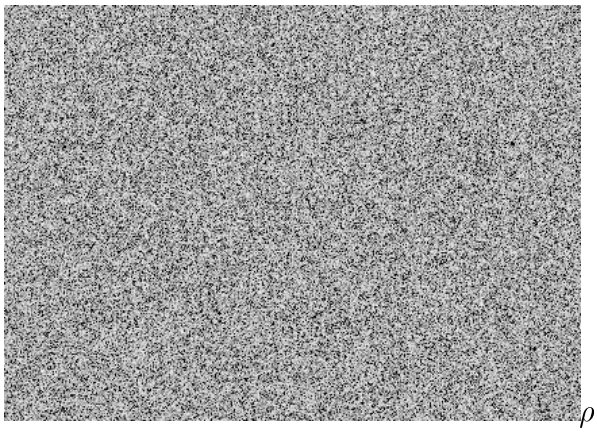

ρ=0.0

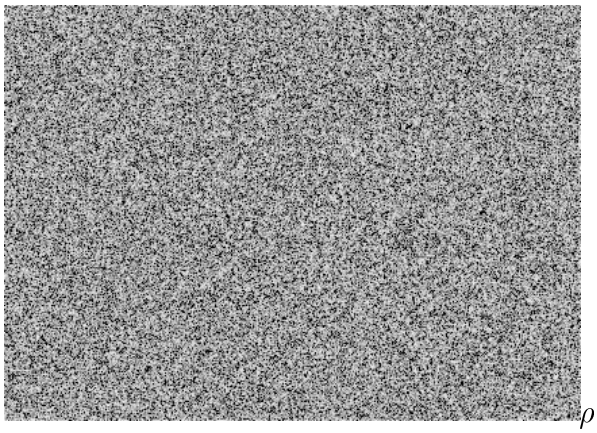

ρ=0.05

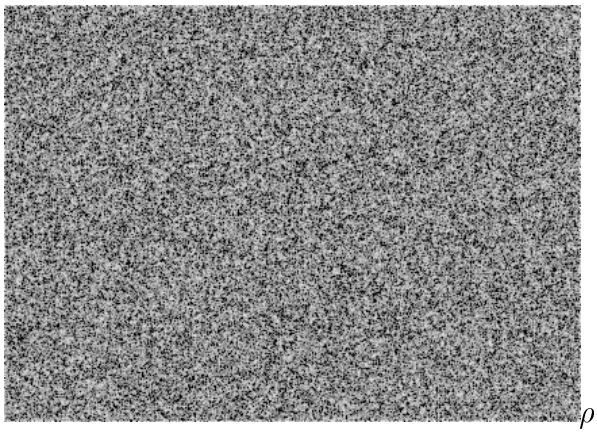

ρ=0.10

FIGURE 4.4. Simulated elevation noise grids for ρ values 0.0, 0.05, and 0.10.

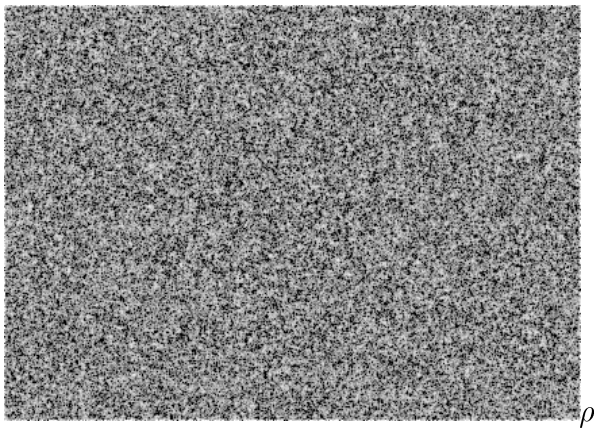

ρ=0.12

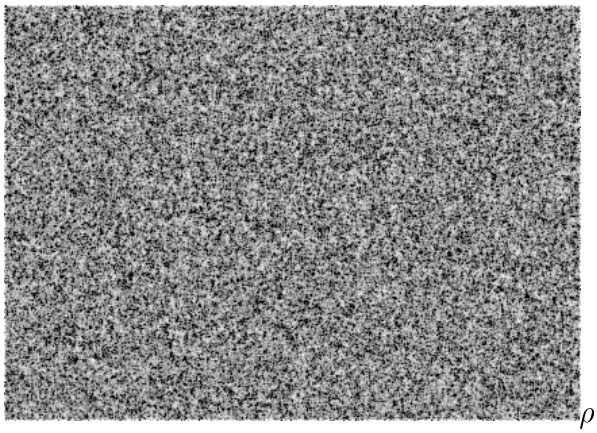

ρ=0.14

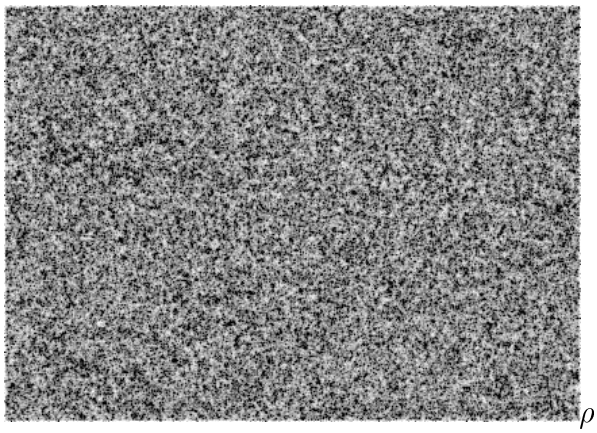

ρ=0.16

FIGURE 4.5. Simulated elevation noise grids for ρ values 0.12, 0.14, and 0.16.

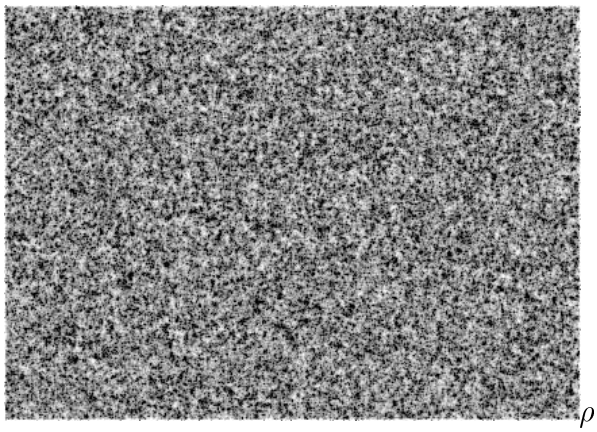

ρ=0.18

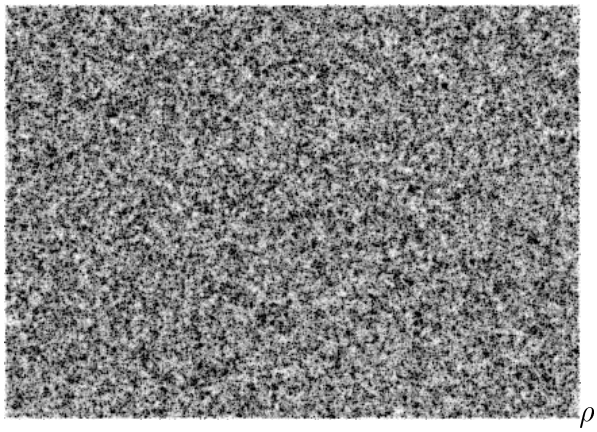

ρ=0.19

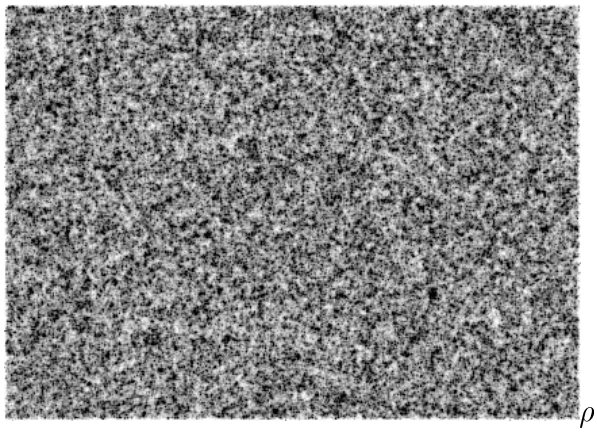

ρ=0.20

FIGURE 4.6. Simulated elevation noise grids for ρ values 0.18, 0.19, and 0.20.

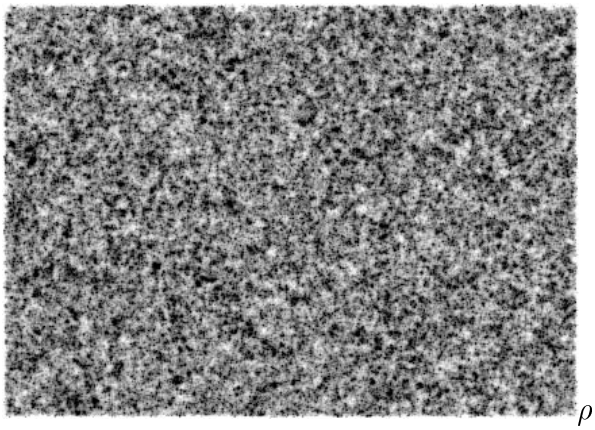

ρ=0.22

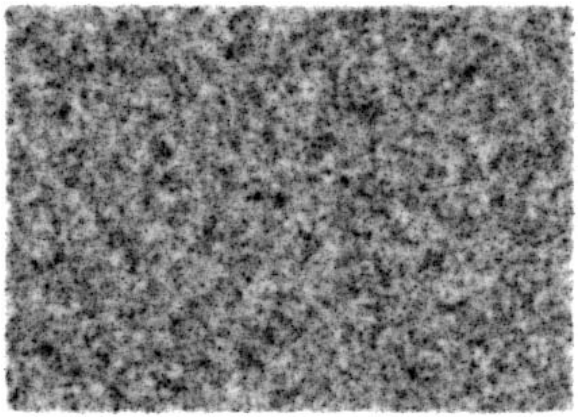

ρ=0.24

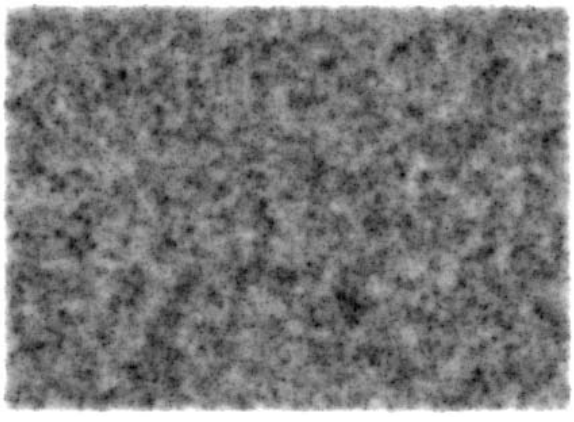

ρ=0.245

FIGURE 4.7. Simulated elevation noise grids for ρ values 0.22, 0.24, and 0.245.

in the absence of other information that suggests a non-zero mean error), and a DEM standard deviation of 7 meters (determined from the USGS estimate of the standard deviation of the error in the DEM), as shown in equation 4.5 (using the ARC/INFO Grid module).

$$grid\_normal = ((error\_grid - mean) * 7))/standard\_deviation\_of\_error\_grid \tag{4.5}$$

Each noise grid is then converted from a floating point grid to an integer grid to permit georeferencing (equation 4.6) to the Andrews Forest boundary. Once georeferenced the noise grids are clipped to the coordinates Andrews Forest boundary using the ARC/INFO LATTICECLIP function. The resulting grids are composed of the parameters determined in stage two (see Table 4.2).

$$grid\_align = shift(integer\_grid, 558946.072, 4893975.967, 30) \tag{4.6}$$

A perturbed version of the DEM is then generated by adding the georeferenced noise grid to the original DEM as shown in equation 4.7 (using the ARC/INFO - GRID module).

$$perturbed\_DEM = (grid\_align + DEM) \tag{4.7}$$

The final debris-slide hazard maps are then created as described in section 4.2.

The last step of stage three is to determine the spatial autocorrelation value to use for the final perturbed debris-slide hazard maps (stage four). This is done by graphing the number of cells with a high slide hazard value in each of the ten final debris slide hazard maps against the 11 ρ values (Figure 4.8). The graph indicates that the number of high values increases slightly from $\rho = 0$ to approximately $\rho = 0.19$, then drops rapidly as ρ approaches 0.25. The value of ρ

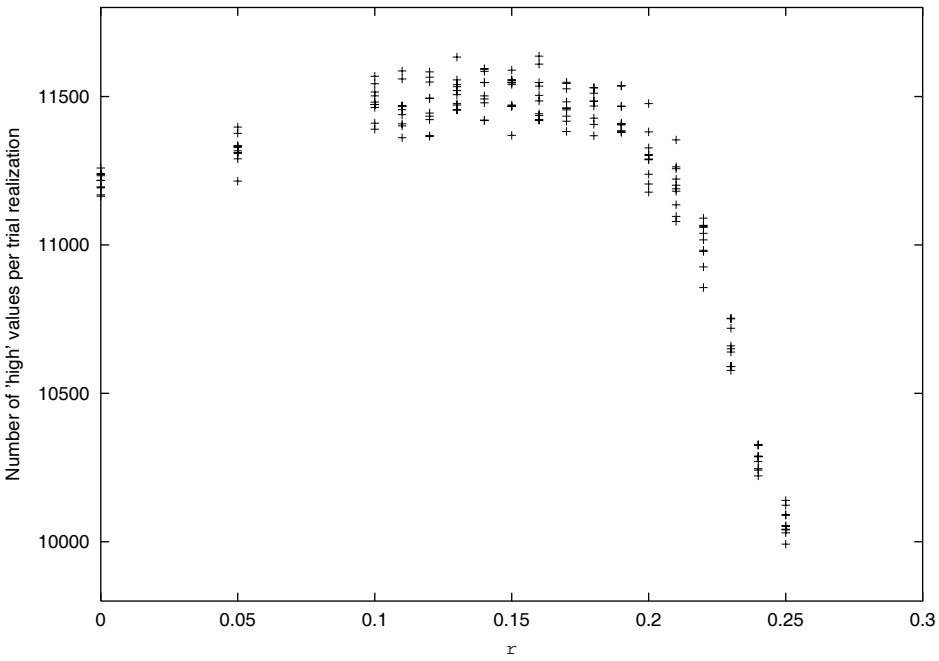

FIGURE 4.8. Graph of the number of cells scoring a 'high' debris-slide hazard rating in each trial perturbed DEM versus variation in the ρ rating.

$= 0.19$ was estimated as the turning point (in terms of ρ) which marks the balance between ensuring that a stochastic approach is in operation yet the results still retain some degree of 'truthfulness' (see section 2.2).

In stage 4 of the uncertainty model this entire procedure was repeated fifty times at the chosen ρ value of 0.19 to produce a set of fifty perturbed debris-slide hazard maps. Figure 4.9 shows a perturbed debris-slide hazard map produced by averaging the fifty maps.

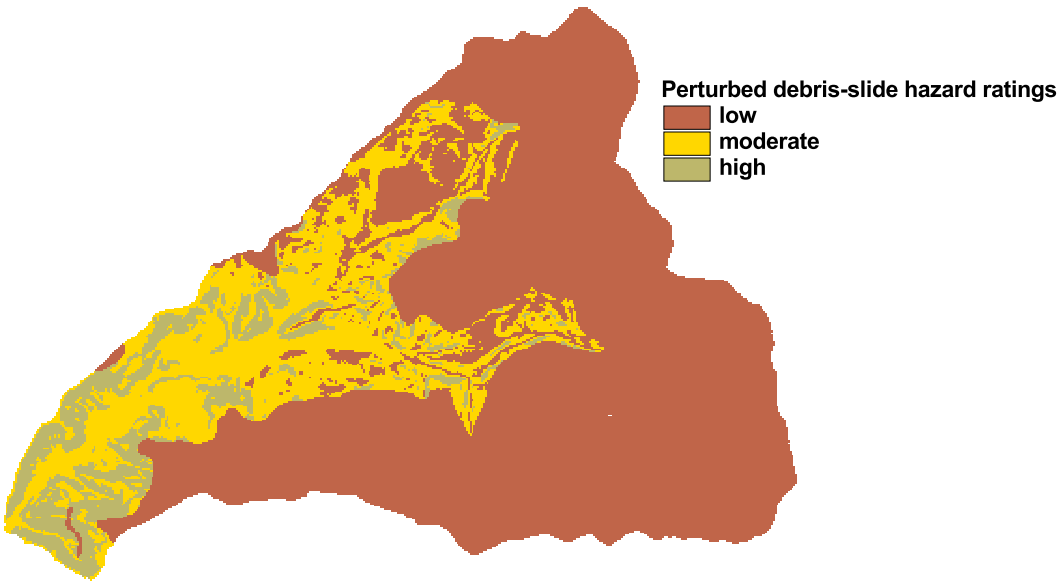

FIGURE 4.9. Perturbed debris-slide hazard map created using a ρ of 0.19.

5. RESULTS

It is believed that the DEM for the Andrews Experimental Forest depicts slope gradients about 10^o less than the field measured values as a result of the tall canopy of dense forest vegetation obscuring the ground surface topography [29]. To validate this difference, the difference between the field and the DEM-derived slopes at each available debris-slide data point were examined. Secondly, all cells in the perturbed debris-slide hazard model were examined to assess the sensitivity of this model to perturbations in the original DEM, and lastly, differences between the original DEM and perturbed DEM debris-slide hazard ratings at each available debris-slide data point were examined. In all cases a general assessment of the data was conducted, and then in order to determine if there was a particular situation in which the data might be more or less sensitive, the analyses were subdivided into two categories: 1) landuse and 2) debris-slide initiation site.

5.1. Field Data

The error associated with the field obtained slopes is unknown, and thus the field measurements cannot necessarily be regarded as true. Additionally, determining what to measure in the field is difficult, for example, should the measurement be at the axis of the sliding surface, or as an approximation of the pre-slide ground surface slope, or the average or maximum of these two? But, we can look at how different the measurement is between field and DEM-derived slopes. The distribution of these differences is plotted in Figure 5.1. The histogram shows a roughly normal distribution, with a mean of -16^o and a standard deviation of 11^o, indicating that on average the slopes at the 145 known debris slides are underestimated by the USGS DEM by approximately 16^o . The minimum (-48.9) and maximum (4.9)

differences indicate some areas are prone to large differences. Overall, ninety-one percent of the field slope measurements are higher than the DEM-derived slope estimates.

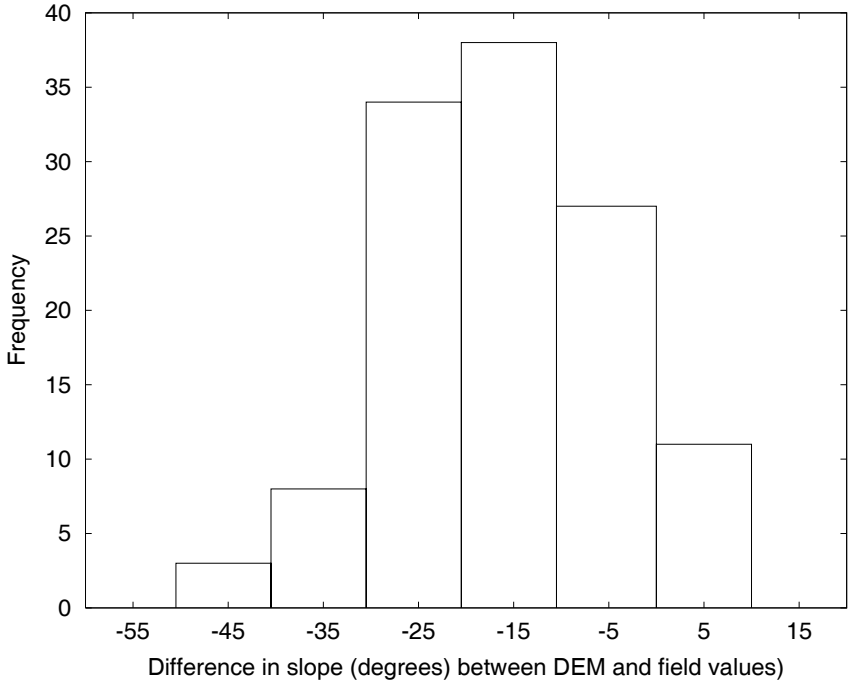

FIGURE 5.1. Histogram of differences between DEM and field slope (^{o}).

Slides in the Andrews Forest area tend to occur on the steepest slopes (approximately 32-40^o), excluding cliffs. Steep microsites where slides initiate are likely to have slope values which are steeper than the mean slope of a 30m x 30m DEM cell that contain the slide site. These results are expected because the field-measured slope value is determined for the axis of the slide scar, which is generally a narrow, steep, linear feature. A DEM slope value is the mean for a 30m x 30m area, which is generally larger and more gently sloping that the axis of the slide scar.

5.1.1. *Debris-Slide Type*

Using the debris-slide location map, the affect of how the coarse resolution of the DEM affects the ability to predict slope was examined for each debris-slide type. For each debris-slide type the difference was calculated by subtracting the field slope from the DEM-derived slope. As expected, the average field measurement is much higher than the average DEM-derived slopes, especially in streamside and streamside-earth sites (Table 5.1). This may be an indication of the inability of the DEM to measure the slope of an event at a smaller scale than the resolution of the DEM. In particular, streamside earthflow slides zone are narrow and bordered by landforms with a gentler slope. That is, the slope of an earthflow is typically less than a non-earthflow hillslope landforms, but where the actual slide is occurring at the streamside edge is steep. Thus, the DEM is measuring a relatively low slope, but the actual slope where the slide occurred is high.

Slide type	Field mean	Field s.d.	DEM mean	DEM s.d.	Diff. in mean
hollow	33.66	7.53	19.99	5.97	-13.67
hillslope	34.96	6.68	22.41	7.5	-14.97
streamside	37	4.39	19.94	6.9	-17.06
s. earthflow	41.45	6.9	16.15	7.38	-25.30

TABLE 5.1. Difference between original DEM and field slope (^{o})

5.1.2. *Landuse Type*

Using the debris-slide inventory map, how the coarse resolution of the DEM might affect the ability to predict slope was examined for each landuse type. For each debris slide in each landuse category the difference was calculated by subtracting the field slopes from the DEM-derived slopes. As expected, the average field slope is much higher than the average DEM-derived slopes, especially in forested areas (Table 5.2). This may be an indication of the source error associated with DEM data collection, in particular recording measurements of the tree height as the elevation instead of the ground elevation. It is also important at this stage to evaluate when maps or photos as sources of the topographic data were made relative to time of logging.

landuse category	Field mean	Field s.d.	DEM mean	DEM s.d.	Diff. in mean
forest	37.02	8.05	18.6	8.21	-18.42
clearcut	36.48	6.4	21.32	6.34	-15.16
road	33.86	5.87	20.97	7.23	-12.89

TABLE 5.2. Summary information for field and DEM slopes (^{o}).

It is evident that the field slopes are much higher overall than DEM-derived slopes, no matter what the landuse category.

5.2. Debris-Slide Hazard Model

5.2.1. *Elevation*

To verify that the error incorporated into the original DEM was stochastic, an elevation difference map (original elevation - perturbed elevation) was produced to visualize the difference in elevation (Figure 5.2). The histogram (Figure 5.3) shows a roughly normal distribution with a mean of -0.13 and a standard deviation of 0.95 meters which is expected as the mean and the standard deviation of the original DEM and the perturbed DEM should be N(0,1) (as dictated by the Uncertainty Model).

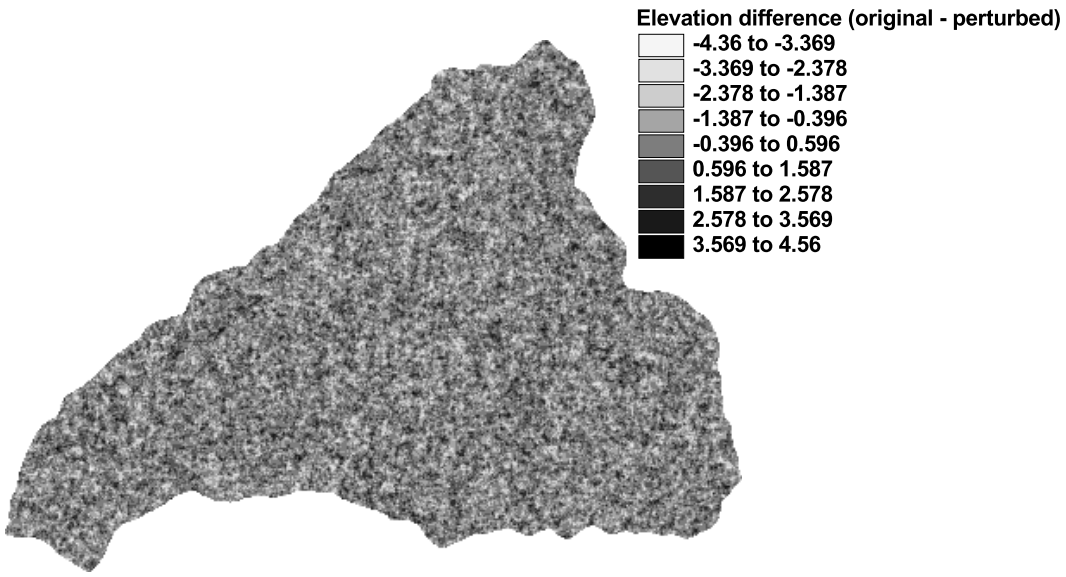

FIGURE 5.2. Elevation difference map for $\rho = 0.19$ (m).

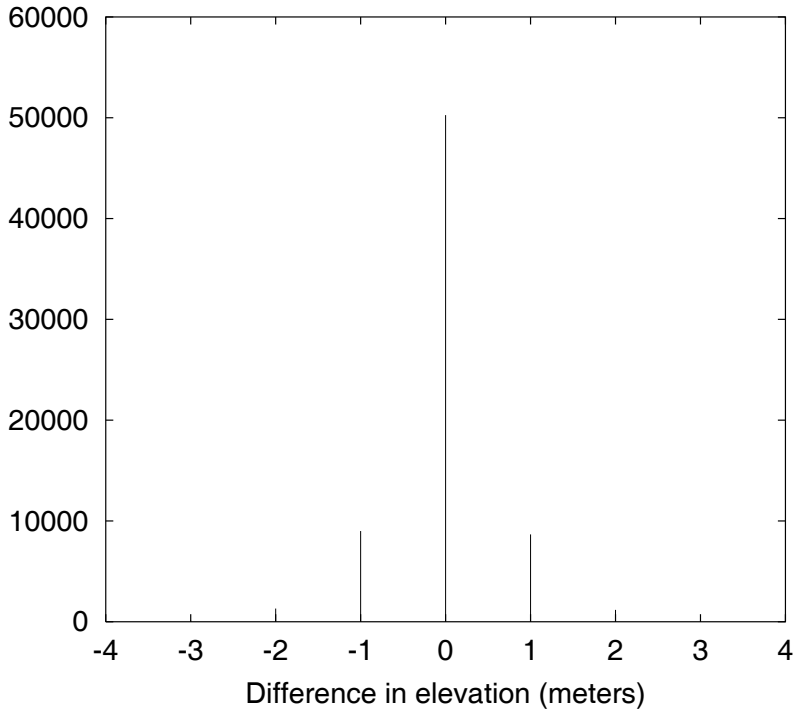

FIGURE 5.3. Graph of Original DEM - perturbed DEM elevation (m).

5.2.2. *Slope*

A single perturbed slope map was created by averaging the 50 perturbed slope maps. While the elevation map indicates no significant trends, the slope difference map (original slope - perturbed slope) map reveals the effect of the introduced error (Figure 5.4). The histogram shows a negatively skewed distribution with a mean of -0.96 and a standard deviation of 1.21 (Figure 5.5). The minimum (-9.5) and the maximum (2.62) indicate that there are definite areas where the perturbed slope is different than the original slope.

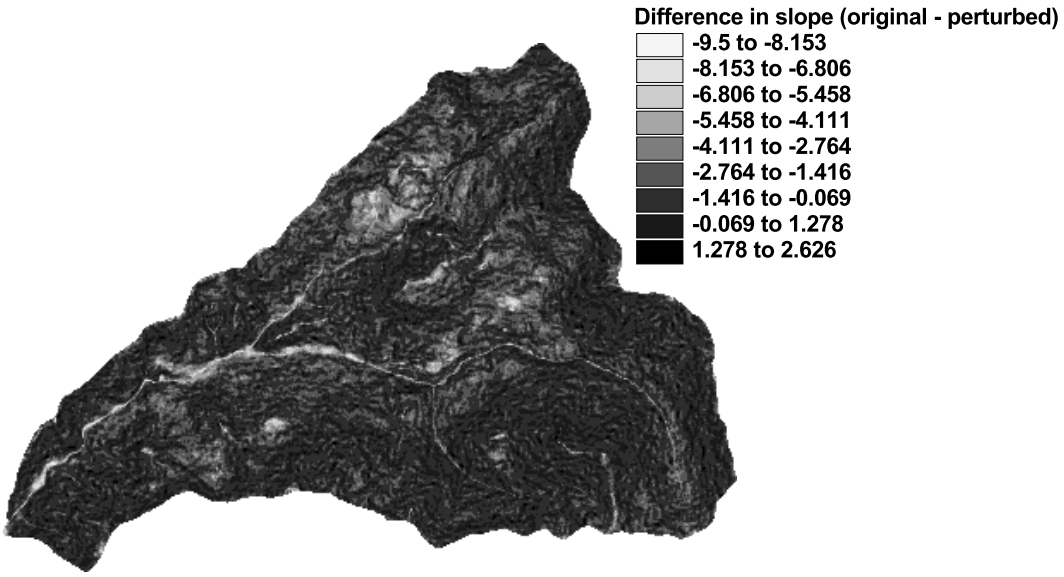

FIGURE 5.4. Slope difference map for $\rho = 0.19$ (^{o}).

The largest negative differences in slopes appear mostly where the slope is $< 10^o$ or in the riparian and stream bed areas. This is a direct result of the slope algorithm used in ARC/INFO as it uses a maximum slope algorithm that prevents a negative slope from being calculated. Thus, if perturbing a set of cells results in a negative slope effectively the algorithm converts it to an absolute

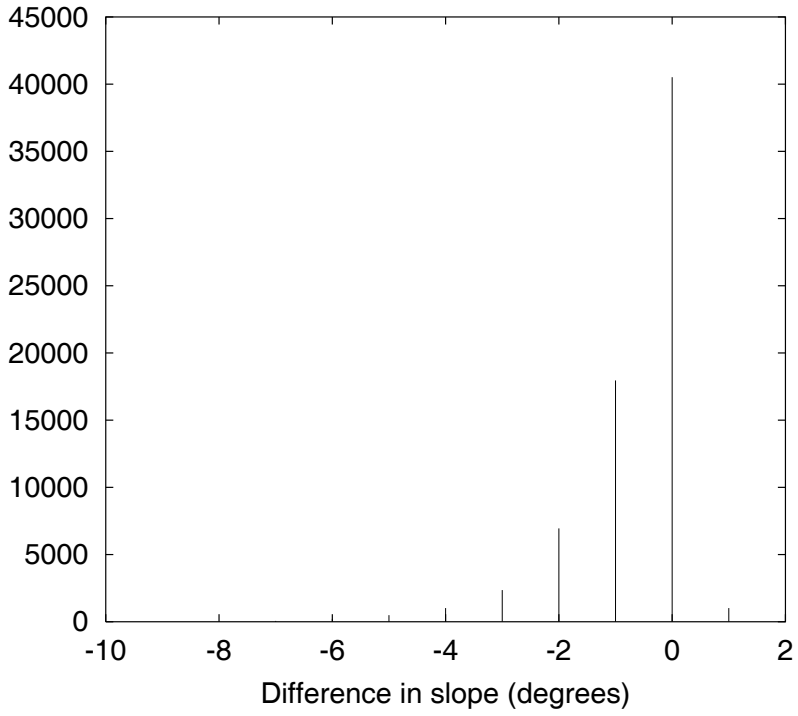

FIGURE 5.5. Graph of original DEM - perturbed DEM slopes(^{o}).

value, thus the perturbed slope will always be higher than the original, resulting in a negative difference. This will occur until the value of the slope is greater than the RMSE divided by 2*Δx at which point there is a 50/50 probability that the slope will increase or decrease. The magnitude of the RMSE also plays a direct role in when the probability of the perturbed slope being higher than the original is 50/50. This hypothesis was tested by developing a simplified model to calculate the slope. Using a 3x3 elevation grid, the slope algorithms from ARC/INFO, a triangular distribution, and by varying the slope in only one direction, the effects of the increase in slope and the magnitude of the RMSE are shown in Figure 5.6. Test runs were made at half the RMSE (0.5*7m) and twice the RMSE (2*7m). In the case of the smaller RMSE, it would be expected that the rate at which the percentage approaches 50% would be higher, as a value of +/- 3m will have even less effect than the 7m. If the RMSE is greater than the +/- 7m, the rate at which the percentage approaches 50% should be reached more slowly than the other two cases. Indeed this is the case as the graph reflects the hypothesis that as slope increases the probability of the perturbed slope being higher than the unperturbed slope asymptotically approaches 50%, and the magnitude of the RMSE affects the rate at which the percentage of perturbed slopes being higher than the unperturbed slopes asymptotically reaches 50%.

5.2.3. *Slope Classes*

The effect of the error seen in the slope is further propagated into the derivation of the slope classes. Figure 5.7 indicates where slope class has changed. The majority of the points do not change (indicated by a slope class difference of 0), but a considerable number of slopes are reclassified into a higher slope class

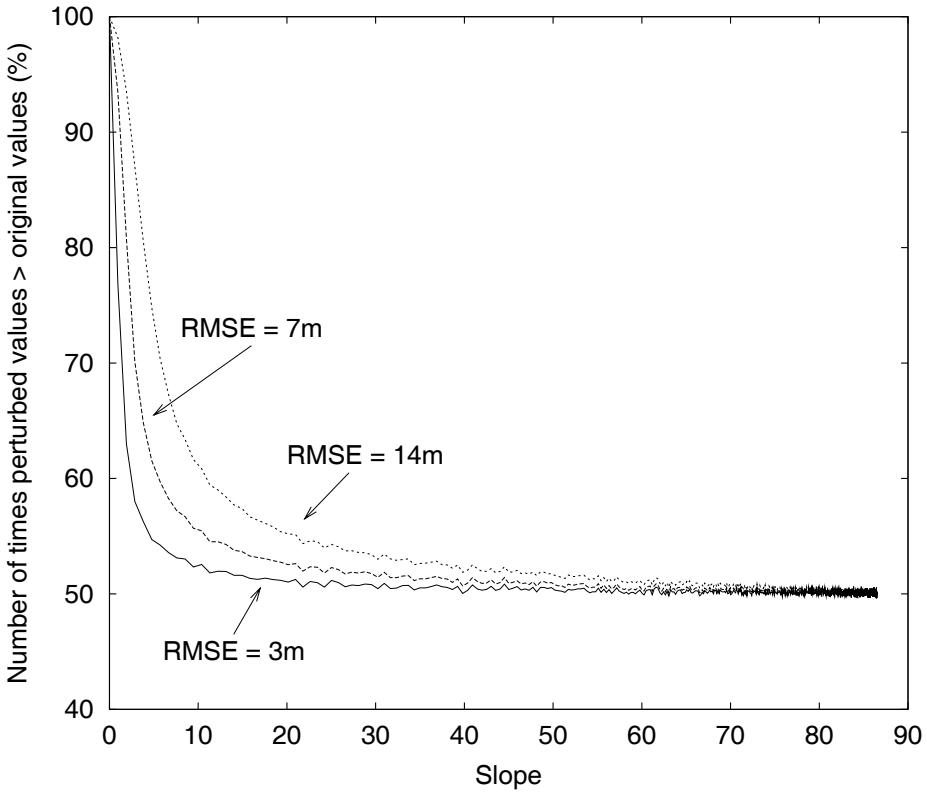

FIGURE 5.6. Probability of the perturbed slope being higher than the unperturbed slope (RMSE = 3, 7, and 14 m).

(indicated by areas with a -1). Very few slopes were reclassified into a lower slope category. As we would expect, the areas most affected are areas of low relief where the slopes are increased due to the perturbations.

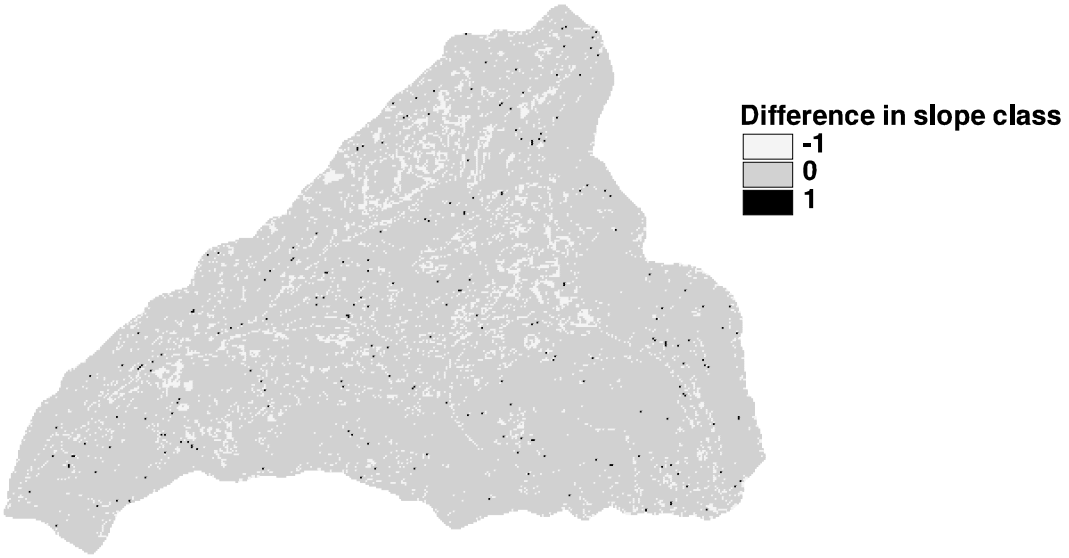

FIGURE 5.7. Difference in original DEM - perturbed DEM slope class.

More detailed information can be determined by using a confusion matrix. A confusion matrix shows the counts of the actual versus predicted values and can show overall how well the model predicts and presents the details needed to see exactly how things have changed. In this case, it can be used to look at the slope classes and the debris slide hazard ratings. In general, the columns represent the unperturbed data, the rows reflect the perturbed data, the cells of the matrix indicate the count of the number of observations for each (column, row) combination. The diagonal elements show agreement between unperturbed and perturbed; a perfect match is indicated by all zero off-diagonals. Errors of omission (discrimination between classes) are calculated by dividing the incorrect in a row by the total in the row. These errors occur when a value is not identified

as belonging to a particular class. Errors of commission (discrimination within classes) are calculated by dividing the incorrect in a column by the total in the column. These errors result when the value is included in another class.

To illustrate how the slope class changes, in Table 5.3, of the 36659 cells classified as steep, 32018 cells were classified as steep in the perturbed slope class map, leaving 12% (4406+145/36659) as the error of omission. Similarly, of the 36659, 3013 cells were improperly classified as moderate or low, producing a commission error of 8% (3013/36659). Of the 36659 cells the percent correctly classified as steep is 88% (32018/36659). Mapping accuracy for each slope class is determined as the number of correctly identified cells, divided by that number plus error cells of commission and omission. The overall map accuracy is determined by summing the diagonal values and dividing by the total number of cells, in this case 73% (32108 + 14919 + 4321)/70026).

The overall trends from the confusion matrix indicate that the likelihood of a cell's debris-slide hazard rating starting out as steep then being reclassified as gentle is small. The same holds true for gentle to steep. However, by being in the middle, a moderate slope class is more likely to be reclassified into either a steep or gentle slope class. The low percentage of accuracy in the gentle (35%) and moderate (44%) reflect the effect of the actual slope (see Figure 5.6) and the ARC/INFO slope calculation algorithms. These two slope class categories appear to have a big impact on the overall accuracy (73%) of the map, as the percentages of omission (12%) and commission error (8%) for the steep class is relatively low.

The percentage of cells in the original DEM likely to be converted into a new slope class category is shown in Table 5.4. As expected, if a cell is classified as steep, there is an 87.7% chance it will remain steep. The steep slope class ranges from 20^o to 65^o, thus, the introduction of error with an RMSE of 7m will not often

Slope Class					
	steep	moderate	gentle	row total	% match
steep	*32108*	4406	145	36659	88%
moderate	6968	*14919*	3864	25752	58%
gentle	252	3617	*4321*	8190	53%
column total	39328	22942	8330	70601	73%

	% omission	% commission	% match
steep	12%	8%	73%
moderate	42%	31%	44%
gentle	47%	49%	35%

TABLE 5.3. Confusion matrix for slope classes.

have an effect. However, lower slopes are more sensitive to the DEM perturbations as only 58.4% of the moderate slopes remain moderate (and both ends of this range are subject to change) and only 54.9% of the gentle slopes remain gentle. In these cases, the RMSE of 7m does affect the resulting slope calculation and a cell is more likely to be reclassified into another slope class category.

While the previous tables show exactly how the error affects each slope class, the overall number of cells that change their slope class is different. Table 5.5 shows the number of cells that were reclassified 'out' of their original class and the number of cells that were reclassified 'in to' their original class. The differences between the two show that there is an overall decrease in the moderate slope category and gains in the steep and gentle slope classes.

Slope Class			
	steep	moderate	gentle
steep	*87.7%*	12.0%	0.39%
moderate	27.3%	*58.4%*	15.1%
gentle	3.2%	45.9%	*54.9%*

TABLE 5.4. Percentage of cells in original DEM likely to be converted into a new slope class category.

Slope Class			
	out	in	difference
steep	4551	7220	+2669
moderate	10832	8023	-2809
gentle	3869	4009	+140

TABLE 5.5. Overall change in number of cells for each slope class

5.2.4. *Debris-Slide Hazard*

As a last step in the model generation, the debris-slide hazard model is created. As expected, the error seen in the slope, and subsequent slope class derivation, propagates into the debris-slide hazard model output. A confusion matrix for the debris-slide hazard rating is shown in Table 5.6.

Slide Hazard					
	high	moderate	low	row total	% match
high	*8574*	1347	26	9947	86%
moderate	2911	*8795*	1205	12912	68%
low	102	1445	*45620*	47167	97%
column total	11587	11587	46851	70026	90%

	% omission	% commission	% match (perturbed matches original)
high	14%	30%	66%
moderate	32%	22%	56%
low	3%	3%	94%

TABLE 5.6. Confusion matrix for debris-slide hazard rating.

Interestingly, the overall accuracy of the perturbed DEM to the original DEM is 90%. This is by virtue of the design of the debris slide hazard model. The high slope class accuracy (94%) for the low debris-slide hazard category results because any cell classified with strong rock characteristics will be classified into the low debris slide category regardless of the slope or slope class. Thus, the perturbation effect on slope and the subsequent slope class derivation does not

alter the low debris-slide hazard category. This in effect aids to raise the overall accuracy percentage.

The 30% commission error in the high debris-slide hazard category, indicates that a large number of slides were classified as high when they should not have been, and the 32% omission error in the moderate debris-slide hazard category indicates that a large number of slides were classified as something other than moderate. Considering the commission and omission percentages for slope class, the actual effect of those errors on the debris-slide hazard model is less than expected. This is a direct result of the structure of the debris-slide hazard model. The stability of the low debris-slide hazard rating (94% slope class accuracy) increases the overall map accuracy to 90% even when the slope class accuracy for high (66%) and low (56%) is relatively low.

While Table 5.6 shows exactly how the error affects slide hazard category, the overall number of cells that change their debris slide hazard class is different. Table 5.7 shows the number of cells that were reclassified 'out' of their original class and the number of cells that were reclassified 'in to' their original class. The differences between the two show that there is an overall increase in the high debris-slide hazard category and a definite loss in the moderate and low debris-slide hazard category.

Similarly, we can look at the percentage of cells in the original DEM that are likely to be converted into a different slide hazard category (Table 5.8). Low and high slide hazard ratings appear to be relatively unaffected by the introduced error, but moderate slide hazard ratings appear to be particularly sensitive to the perturbations. As described earlier, by virtue of the design of the slope hazard model it is unlikely that a cell classified as low will be reclassified into high, and only a small chance it will be reclassified into a moderate slide hazard as this can

Slide Hazard			
	out	in	difference
high	1373	3013	+1640
moderate	4116	2792	-1324
low	1547	1231	-316

TABLE 5.7. Overall change in number of cells for each debris slide hazard category.

only occur when the cell is in the moderate geologic stability category. Similarly, it is unlikely that a high debris-slide hazard will be reclassified into a low debris-slide hazard category, but with a slightly higher chance at being reclassified as a moderate slide hazard (cells classified in either the moderate or the weak geology category can be reclassified into the moderate debris-slide hazard category). Thus, the percentages seen in Table 5.8 reflect not only the perturbations introduced into the DEM, but the design and structure of the debris slide hazard model.

To get an idea of how the overall area of each debris-slide category is affected by the introduction of perturbations, the percentage of area affected by the random perturbations is shown in Table 5.9. The original debris-slide hazard model predicts a 2.3% smaller area will fail than does the perturbed debris-slide hazard model. Conversely, the area classified as having a moderate debris-slide hazard potential is underestimated by the perturbed debris-slide hazard model by 1.8%.

Slide Hazard			
	high	moderate	low
high	*86.2%*	13.5%	0.3%
moderate	22.6%	*68.1%*	9.3%
low	0.2%	3.1%	*96.7%*

TABLE 5.8. Percentage of cells in original DEM likely to be converted into a new slide hazard category.

Area affected			
Slide hazard	Original	Perturbed	Difference
high	14.2%	16.5%	-2.3%
moderate	18.3%	16.5%	1.8%
low	67.4%	66.9%	0.5%

TABLE 5.9. Percentage of area in each debris-slide hazard for both original and perturbed.

5.2.5. *Scoring*

One last method to determine the overall sensitivity of the model is to use a method of 'scoring.' Each cell in the debris-slide hazard map is assigned an attribute of 'high.' If a cell was classified as having a high debris-slide rating, it was assigned a value of 1, if not, it was assigned a 0. This was done in the original debris-slide hazard map and for the each of the 50 perturbed debris-slide hazard maps. The 50 perturbed debris-slide hazard maps were then added together using only the 'high' classification. That is, the resulting cell value attribute of 'high' denoted the number of times each cell scored a high rating in the range of 0-50.

In order to visualize the results, the original hazard map was overlaid with all grid cells with a high hazard rating for the study site (Figure 5.8). For comparison, cells that scored a high rating at least once (Figure 5.9), together with those that achieved the maximum score of 50 (Figure 5.10) were shaded black and overlaid on the same map.

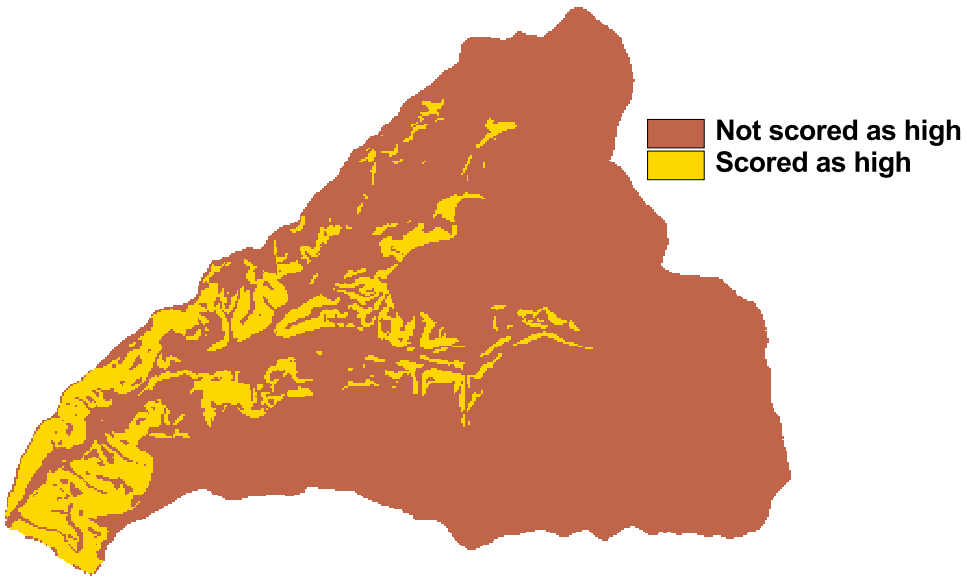

FIGURE 5.8. Original hazard map scoring a 'high' hazard rating.

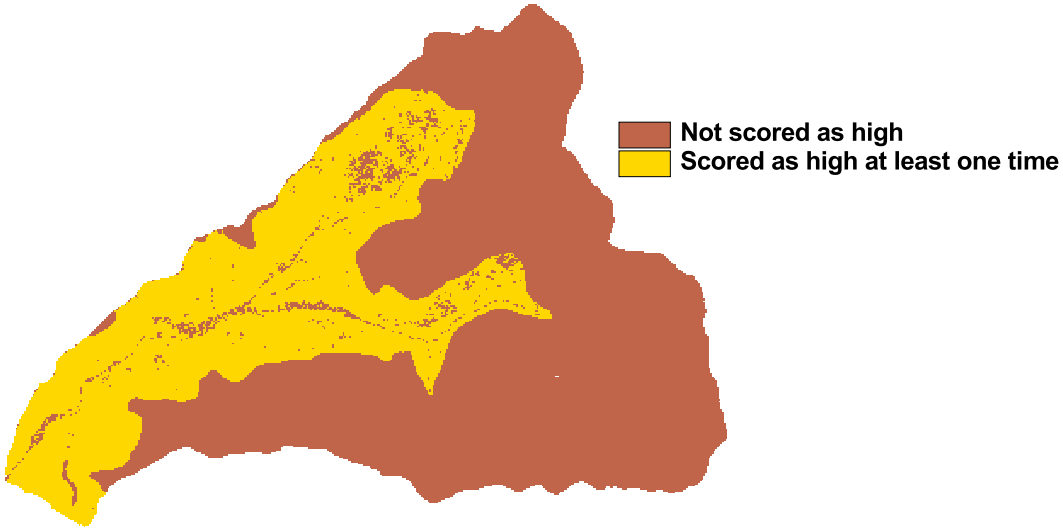

FIGURE 5.9. Perturbed (ρ=0.19) debris-slide hazard map indicating where a 'high' debris-slide hazard rating was 'scored' at least one time.

In the original debris-slide hazard map, the Boolean nature of the slope reclassification into categories with thresholds at 10 and 20 meant that a cell could receive only one rating. However, with the proposed method, even though the same thresholds are maintained (and their values are not in question here), we can see how the hazard rating for a cell behaves under variation of the input DEM. Obviously, cells lying on weak or moderate rock and having slope gradients close to either of the thresholds are most likely to exhibit variation in their hazard. The number of high cells in the original debris-slide map and the area of test site affected are compared with the number of cells achieving a high score between 0-50 in the cumulative realized grids (Table 5.10).

5.3. Debris-Slide Inventory Sites

The debris-slide point map was used to examine if any particular areas could be determined as being more sensitive to the elevation perturbations. An

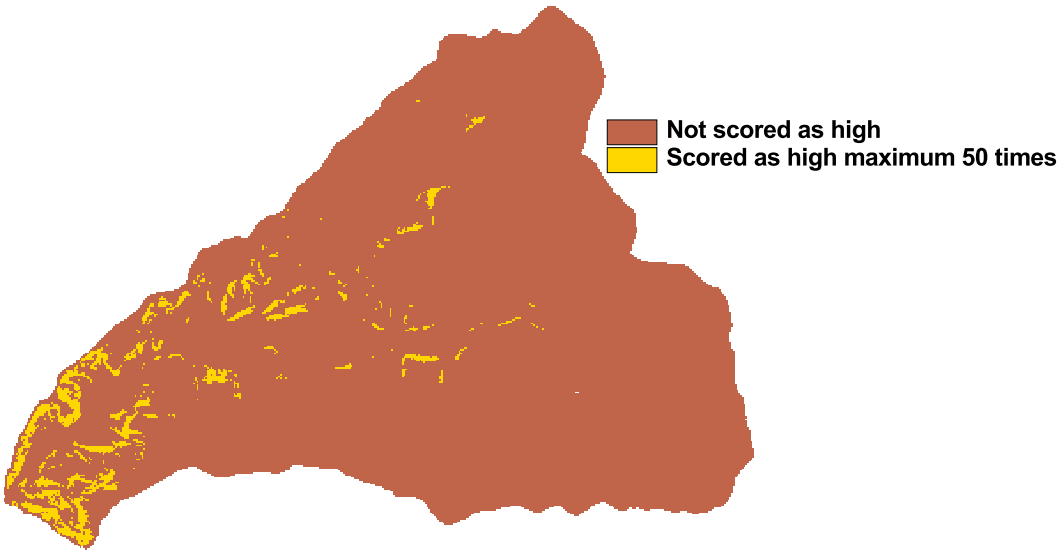

FIGURE 5.10. Perturbed (ρ=0.19) debris-slide hazard map indicating where a 'high' debris-slide hazard rating was 'scored' the maximum 50 times.

High score	No. of cells	Area of site	Site area (ha)
0	24477	36%	2203
≥ 1	22982	33%	2068
≥ 10	15937	23%	1434
≥ 20	12087	17%	1088
≥ 30	9336	13%	840
≥ 40	6723	9.6%	605
50	2583	3.7%	232
Original DEM	9947	14%	895

TABLE 5.10. Relationship between 'high' hazard cell scores and the area of the site affected.

overall summary of the 145 points is shown in a confusion matrix (Figure 5.11). In the case of just these 145 points, none of the high debris-slide hazard cells were reclassified, only a few of the low, and a large number of the moderate.

Slide Hazard					
	high	moderate	low	row total	% match
high	*51*	0	0	51	100%
moderate	19	*42*	0	61	69%
low	0	6	*27*	33	82%
column total	70	48	27	145	83%

	% omission	% commission	% match
high	0%	37%	73%
moderate	31%	10%	63%
low	18%	0%	82%

TABLE 5.11. Confusion matrix for slide hazard rating using the debris-slide hazard points.

5.3.1. *Debris-Slide Type*

To explore the idea that land use at the debris-slide initiation site may affect how well the DEM estimates slope, the mean slope in each category of debris-slide initiation site was calculated (Table 5.12). The perturbed slopes are higher than the original slopes. Streamside and streamside earthflow slides appear to be the most affected. These type of slides are much smaller than hollow or hillslope type slides, and the ability of the DEM to determine the slope at these microsites is

limited. Additionally, the slope of the adjacent landforms factor into the slope calculation (see Section 5.1.1).

Slide type	Pert. mean	Pert. s.d.	DEM mean	DEM s.d.	Diff. in mean
hollow	20.6	5.96	19.81	6.61	-0.79
hillslope	23.2	7.35	22.5	7.87	-0.70
streamside	21.66	6.72	20.78	7.49	-0.88
s. earthflow	16.7	6.7	15.27	7.54	-1.43

TABLE 5.12. Mean slope for each debris-slide initiation site category (^{o}).

The overall change in the 145 points is shown in (Table 5.13). It reflects the pattern seen in the overall debris-slide hazard model.

Slide Hazard			
	out	in	difference
high	0	15	+15
moderate	15	6	-9
low	6	0	-6

TABLE 5.13. Overall change in number of cells for each debris-slide hazard category.

Confusion matrices were made for each debris-slide initiation site (Tables 5.14, 5.15, 5.16, and 5.17). Streamside and streamside earthflow slide sites have the lowest overall percentage of matching between the perturbed and the original

slide hazard value while hollow and hillslope fare well. In each category all slides in the high slide hazard category were correctly matched (100%). This is most likely due to the fact that very few points were reclassified into a lower slope class category because of the slope algorithm or because the slope was much greater than 20^o. However, the lower percentage match values that incorporate omission and commission errors for the high and moderate slide category reflect the tendency of the cells to be reclassified into a higher slope category.

Slide Hazard: streamside sites					
	high	moderate	low	row total	% match
high	*7*	0	0	7	100%
moderate	6	*5*	0	11	45%
low	0	2	*3*	5	60%
column total	13	7	3	23	65%

	% omission	% commission	% match
high	0%	86%	54%
moderate	55%	18%	38%
low	40%	0%	60%

TABLE 5.14. Confusion matrix for debris-slide hazard rating at streamside slide sites.

Slide Hazard: streamside earthflow sites					
	high	moderate	low	row total	% match
high	*5*	0	0	5	100%
moderate	1	*13*	0	14	93%
low	0	3	*0*	3	0%
column total	6	16	0	22	82%

	% omission	% commission	% match
high	0%	20%	83%
moderate	7%	21%	76%
low	100%	0%	0%

TABLE 5.15. Confusion matrix for debris-slide hazard rating at streamside earthflow slide sites.

Slide Hazard: hillslope sites					
	high	moderate	low	row total	% match
high	*24*	0	0	24	100%
moderate	6	*8*	0	14	57%
low	0	0	*9*	9	100%
column total	30	8	9	47	87%

	% omission	% commission	% match
high	0%	25%	80%
moderate	43%	0%	57%
low	0%	100%	100%

TABLE 5.16. Confusion matrix for debris-slide hazard rating at hillslope slide sites.

Slide Hazard: hollow sites					
	high	moderate	low	row total	% match
high	*7*	0	0	7	100%
moderate	2	*8*	0	10	80%
low	0	1	*11*	12	92%
column total	9	9	11	29	87%

	% omission	% commission	% match
high	0%	29%	78%
moderate	20%	10%	73%
low	8%	0%	92%

TABLE 5.17. Confusion matrix for debris-slide hazard rating at hollow slide sites.

5.3.2. *Landuse Type*

To explore the idea that debris-slide initiation site may affect how well the DEM estimates the slope, the mean slope in each category of landuse type was calculated (Table 5.18). As has been the pattern thus far, the perturbed slopes are higher than the original slopes. Forested and roaded areas indicate more of a difference than clearcut. This may be due to an artificial flattening of the elevation, that is, in a forested area the tree height is often misread as the true elevation and would appear flatter than the actual ground gradient.

Slide type	Pert. mean	Pert. s.d.	DEM mean	DEM s.d.	Diff. in mean
Forest	19.78	7.65	18.8	8.46	-0.98
Clearcut	21.58	6.58	20.79	7.09	-0.79
Road	23.17	7.38	22.22	8.29	-0.95

TABLE 5.18. Mean slope for each landuse category (^{o}).

The overall change in the 145 points is shown in (Table 5.19). It reflects the pattern seen in the overall debris slide hazard model.

Slide Hazard			
	out	in	difference
high	0	19	+19
moderate	19	6	-13
low	6	0	-6

TABLE 5.19. Overall change in number of cells for each debris-slide hazard category.

Confusion matrices were made for each landuse type. (Tables 5.20, 5.21, and 5.22). In clearcut and roaded areas moderate slide hazard is most affected. In forest areas low slide hazard areas are most affected. In each category all slides in the high slide hazard category were correctly matched (100%). This is most likely due to the fact that very few points were reclassified into a lower slope class category because of the slope algorithm or because the slope was much greater than 20^o. However, the lower percentage match values that incorporate omission and commission errors for the high and moderate slide categories reflect the tendency of the cells to be reclassified into a higher slope category.

Slide Hazard: forest sites					
	high	moderate	low	row total	% match
high	*14*	0	0	14	100%
moderate	6	*23*	0	29	89%
low	0	4	*9*	13	69%
column total	20	27	9	56	82%

	% omission	% commission	% match
high	0%	43%	70%
moderate	21%	14%	70%
low	31%	0%	69%

TABLE 5.20. Confusion matrix for debris-slide hazard rating at forest sites.

Slide Hazard: clearcut sites					
	high	moderate	low	row total	% match
high	*25*	0	0	25	100%
moderate	10	*16*	0	26	62%
low	0	1	*12*	13	92%
column total	35	17	12	64	83%

	% omission	% commission	% match
high	0%	25%	80%
moderate	50%	17%	43%
low	14%	0%	86%

TABLE 5.21. Confusion matrix for debris-slide hazard rating at clearcut sites.

Slide Hazard: road sites					
	high	moderate	low	row total	% match
high	*12*	0	0	12	100%
moderate	3	*3*	0	6	50%
low	0	1	*6*	7	92%
column total	15	4	6	25	84%

	% omission	% commission	% match
high	0%	40%	71%
moderate	38%	4%	59%
low	8%	0%	92%

TABLE 5.22. Confusion matrix for debris-slide hazard rating at roaded sites.

6. DISCUSSION AND CONCLUSIONS

In this study, a process has been described whereby a simple model used in identifying areas susceptible to landslides with the aid of a GIS has been modified to assess the uncertainty in the final debris-slide hazard map as a result of elevation error in the original DEM and its propagation effects upon the intermediate processes involved. Several different, but equally probable, versions of the input DEM were created through the addition of random, spatially autocorrelated noise (error) files, and then processed to produce a family of landslide susceptibility maps. By examining the resulting output for each grid cell, users may then evaluate the spatial variation in uncertainty throughout the data set.

There are two benefits to the research. Firstly, the inclusion of uncertainty assessment in the process has the potential to facilitate improved land management decisions in relation to timber harvesting in regions susceptible to landslides. And secondly, the application of the uncertainty model to applications such as that described here provides a new approach to understanding the quality of our geographic information and its inherent strengths and weaknesses.

6.1. Summary of Results

Results from this study show that error affects this slide model in two particulars ways. Low relief areas are heavily affected by the slope algorithm used in ESRI's ARC/INFO, and moderate and high relief areas are particularly affected by the structure of the debris-slide hazard model.

6.1.1. *Algorithm and RMSE Effects*

Slopes on the order of the RMSE divided by 2*Δx are most likely to increase when the DEM is perturbed. This occurs in part because the slope algorithm used prevents the calculation of a negative slope by squaring the slope. As the slope increases, on average, the effect of the RMSE is negligible and the likelihood that the perturbed slope will be higher than the original slope is the same as the likelihood it will be smaller. Additionally, the rate at which the probability of the perturbed slope being higher than the original slope approaches 0.50 is correlated to the RMSE value. The lower the value of the RMSE the quicker it's affect is lost and the subsequent corresponding slope value is lower. Conversely, the slope value at which point the probability is approximately 0.50 becomes higher at the RMSE increases. Thus, the algorithms, the source error, and their subsequent interactions should be examined when modeling with a GIS.

6.1.2. *Debris-Slide Model Effects*

The derivation of the debris-slide categories and its effect on the perturbed output is evident. The perturbed slope class cell values matched the original slope class cell values approximately 73% of the time. Yet, the percentage of matching debris-slide hazard values between the perturbed and original is relatively high, i.e. 90%. This is directly related to the derivation of the debris-slide model. In the case of the strong bedrock category, any change in slope class does not produce a change in the hazard rating. In this case, no matter the slope class, the slide hazard rating will be classified as low. The most change will be seen in the moderate bedrock category. This is the only case in which a change in slope class will produce a change in the slide rating every time and also the only time a change in slope

class can potentially lead a cell to be reclassified into a low slide hazard category. The last bedrock category, weak, allows only change from a moderate to high slide rating and vice-versa. The other interesting effect, is that if a cell changes from slope class moderate to gentle, or gentle to moderate, no change in slide hazard will occur. The only time a hazard rating change will occur is when cells with a steep rating are reclassified into a lower slope class, or when cells with a moderate or gentle slope class rating are reclassified into the steep category.

Lastly, because the model uses slope classes and not the slope itself, once the slope is greater than 20^o +RMSE, the effect of error is negligible. That is, if a slope is 45^o, with the RMSE of 7m, the ability to perturb the elevation such that the slope value will be less than 20^o is not likely. Thus, any perturbation to elevation will permit large slope values to remain in the same slope class category as in the original model output.

6.1.3. *Landuse and Slide Initiation Site*

Streamside slide sites exhibited a tendency to be more affected by the perturbation of the DEM, however, in general the points used reflect the patterns seen in the entire debris-slide map.

6.2. Scale Issues

In this study, scale plays a very important role. The scale of the DEM, of the RMSE (as mentioned above), of the landscape feature being interpreted, and of the products all can affect the output of this model. For example, there are currently available finer-resolution and higher accuracy DEMs (e.g. LIDAR). How

one of these DEMs would be behave in a process similar to the one used in this study opens a whole new set of questions and is an area for further research.

6.3. Uncertainty Model Implications

From a land management perspective, where areas susceptible to debris slides are to be protected from harvesting, selecting all cells that achieve a high hazard rating at least once is clearly the most cautious approach. This leads to an overestimation of the true area where the model predicts high slide potential. On the other hand, selecting only those cells that attain a high score the maximum 50 times is the least cautious approach and more than likely underestimates the true area of the site susceptible to debris slides.

Clearly there is no right or wrong answer to the selection problem, and the level of risk a user is prepared to accept in the end product is a matter of institutional and/or personal choice. In other words, users must live with some degree of uncertainty in their geographic information outputs and make value judgments according to individual project requirements. In circumstances where several parties with opposing views are involved in land management decisions, it may be more appropriate to adopt a compromise value (verified by random field checks) such as grid cells that score a high debris-slide hazard index 40 out of 50 times are to be protected from harvesting and road construction, and in this way a measure of uncertainty can be introduced to the decision making process based on the uncertainty associated with the GIS outputs. Of course, the process adopted here could also be applied to test the effects of uncertainty in source data sets.

Finally, positional uncertainty in the geological boundaries used to interpret rock strength is another error source which affects the hazard index. At this stage,

the uncertainty model described here is not capable of handling this aspect since a solution requires perturbation of the original vector-based geological polygon boundaries. However, research is currently being conducted in this area and Hunter et. al. [30] describe the experimental work that has been done to date to overcome the problem.

The potential of this model lies in four areas [28]. First, regions of maps may be highlighted to represent areas susceptible to change in parameter values. For instance, Hunter and Goodchild [11] showed that slope aspect calculations from the DEM were susceptible to variations in elevation in relatively flat terrain while steep hillslopes remained relatively stable. Additionally, parameter value differences could be used for input to a sensitivity analysis to study the effects on the decision making process, as in landuse suitability and capability studies.

Second, the technique is also useful in cases where differences may not be as important as determining the particular class in which a cell resides. For example, one might calculate which cells are visible or invisible from a particular viewing point in a viewshed computation.

Third, a reverse engineering approach might be applied to areas identified on a map that exhibit unacceptable levels of uncertainty. This process begins by applying various techniques of uncertainty reduction (e.g. recollecting data at a higher accuracy) to the data contained within the questionable areas. The uncertainty model can then be applied to the modified maps to determine the effect of the uncertainty reduction technique on the final outcome, before one returns to the field site or purchases an alternative data set. Finally, one may wish to compare several realizations of a map to study the amount of variation associated with the processes of interest. For example, several realizations can be produced to assess the impact of a raster-to-vector conversion, such as deriving contour lines from a

DEM. In this case, the impact of elevation uncertainty and the variation due to the contour line interpolation process can be determined.

6.4. Future Uncertainty Models

The uncertainty model discussed thus far only considers raster or grid data. Spatial data are also available in vector form and are susceptible to many of the same errors and uncertainty as raster data. An experimental uncertainty model for vector data has been proposed by Hunter et. al. [30]. This technique is based on the same principles as the raster model. If one assumes that, within a vector data set, any error or uncertainty possesses a circular normal distribution (defined earlier see section II.3.A), and that the x and y vector components are independent, it is possible to combine the original data set with a set of positional error vectors to create a new, but equally probable, description of the data. This is accomplished by the creation of two independent, normally distributed, error grids, one for each of the x and y component directions. These perturbed grid data sets are constructed based on control information, such as residuals at control points obtained in the digitization process or data quality information furnished with topographic or resource data. Combining these perturbations with the original data set (via the GIS OVERLAY function) results in the creation of a distorted output data set, i.e., a set consisting of the data (x + uncertainty, y + uncertainty).

This perturbation process is performed in a consistent manner, with the error grids consisting of normally distributed values with a mean and standard deviation corresponding to the horizontal error estimate of the original data set (i.e., from the topographic description). In this process, it is necessary to employ spatial autocorrelation to avoid an inconsistent result. As an example, consider the

case in which the perturbation of neighboring cell data is in opposite directions. If the perturbation magnitude is large, it is possible to actually interchange the source cell data between the two neighboring cells in the output. This situation will create extreme, undesirable distortions or transpositions of the features in the data set. The grid point separation distance may be selected arbitrarily. However, it should not be larger than the smallest x or y distance that describe the features in the original data.

6.5. Conclusion

This study indicates that when using GIS even uncertainty can be considered with scrutiny, a certain amount of rigor, and understanding. The ease in which data can now be downloaded, stored, and manipulated leads to many steps in the process for introduced error and subsequently propagated error. Users must live with some degree of uncertainty in their geographic information and decide what level of error they are willing to accept. This may be dependent on the project, time, or finances. To aid in these decisions any type of uncertainty analysis has the potential to make any GIS analysis more robust and at least associate the amount of error or uncertainty associated with the output.

BIBLIOGRAPHY

[1] D.N. Swanston. Slope stability problems associated with timber harvesting in mountainous regions of the western United States, 1974.

[2] Swanston D.N. and F.J. Swanson. Timber harvesting, mass erosion, and steepland forest geomorphology in the Pacific Northwest. In D.R. Coates, editor, *Geomorphology and Engineering*, pages 199–221. 1976.

[3] Amaranthus M. P. Rice R. M. Barr N.R. and R. Ziemer. Logging and forest roads related to increased debris slides in southwestern Oregon. *Journal of Forestry*, 83(4):229–233, 1987.

[4] F.J. Swanson, M.M. Swanson, and C. Woods. Analysis of debris-avalanche erosion in steep forest lands: An example from Mapleton, Oregon, USA. In Davies T.R.H. and Pearce A.J., editors, *Proceedings Symposium on Erosion and Sediment Transport in Pacific Rim Steeplands*, pages 67–75. IAHS-AISH, Christchurch, 1989.

[5] Swanson F.J and G.W. Lienkaemper. Geologic zoning of slope movements in western Oregon, USA. In *Proceedings of the 5th International Conference and Field Workshop on Landslides*, pages 41–45, 1985.

[6] J McKean, Buechel S., and L. Gaydos. Remote sensing and landslide hazard assessment. *Photogrammetric Engineering and Remote Sensing*, 57(9):1185–1193, 1991.

[7] Skaugset A. Slope stability and general hydrology research. Forest Soils and Riparian Zone Management: The Contributions of Dr. Henry A. Froehlich to Forestry, 1992.

[8] H. Veregin. Developing and testing of an error propagation model for GIS overlay operations. *International Journal of Geographical Information Systems*, 9(6):595–619, 1995.

[9] Goodchild M.F. Guoqing S. and Y. Shiren. Development and test of an error model for categorical data. *International Journal of Geographical Information Systems*, 6:87–104, 1992.

[10] G.J. Hunter and M.F. Goodchild. A methodology for reporting uncertainty in spatial databases products. *Journal of the Urban and Regional Information Systems Association*, 7, 1995.

[11] G.J. Hunter and M.F. Goodchild. Modeling the uncertainty of slope gradient and aspect estimates in spatial databases. *Geographical Analysis*, 29:35–59, 1996.

[12] Swanson F.J. and M. E. James. Geology and geomorphology of the H.J. Andrews Experimental Forest, western Cascades, Oregon, 1975.

[13] Dyrness C.T. Mass soil movements in the H.J. Andrews Experimental Forest. Pacific Northwest Forest and Range Experiment Station Research Paper, 1967.

[14] Swanson F.J. and Dyrness C.T. Impact of clearcutting and road construction on soil erosion by landslides in the western Cascade range, Oregon. *Geology*, 3:393–396, 1975.

[15] Goodchild M. F. and O. Dubuc. A model of choroplethic maps, with applications to geographic information systems. *Auto Carto 8 Proceedings*, pages 165–174, 1987.

[16] P.A. Burrough. *Principles of Geographic Information Systems for Land Resources Assessment*. Clarendon Press, Oxford, 1986.

[17] G. Maffini, M. Arno, and W. Bitterlich. Observations and comments on the generation and treatment of error in digital GIS data. In M.F. Goodchild and S. Gopal, editors, *Accuracy of Spatial Databases*. Taylor and Francis, London, 1989.

[18] P.F. Fisher. Modeling soil map-unit inclusions by Monte Carlo simulation. *International Journal of Geographic Information Systems*, 5(2):193–208, 1991.

[19] K. Thapa and J. Bossler. Accuracy of spatial data in geographic information systems. *Photogrammetric Engineering and Remote Sensing*, 58(6):835–841, 1992.

[20] I. Heyword, S. Cornelius, and S. Carver. *An Introduction to Geographical Information Systems*. Addison-Wesley Longman, New York, 1998.

[21] H. Veregin. Integration of simulation modeling and error propagation for the buffer operation in GIS. *Photogrammetric Engineering and Remote Sensing*, 60(4):427–435, 1994.

[22] R.S. Lunetta, R.G. Congalton, L.K. Fenstermaker, J.R. Jensen, K.C. McGwire, and L.R. Tinney. Remote sensing and geographic information system

data integration; error sources and research issues. *Photogrammetric Engineering and Remote Sensing*, 57(6):677–687, 1991.

[23] N.R. Chrisman. Modeling error in overlaid categorical maps. In M.F. Goodchild and S. Gopal, editors, *Accuracy of Spatial Databases*. Taylor and Francis, London, 1989.

[24] M.F. Goodchild. Data models and data quality: Problems and prospects. In M.F. Goodchild B.O. Parks and L.T. Steaert, editors, *Environmental Modeling with GIS*, pages 94–103. 1993.

[25] A.D. Cliff and K.K. Ord. *Spatial Processes: Models and Applications*, page 147. Pion, London, 1981.

[26] H. Veregin. A taxonomy of error in spatial databases. Technical Report 89-12, National Center for Geographic Information and Analysis, Santa Barbara, CA, 1989.

[27] J.R. Carter. Relative errors identified in USGS gridded DEMs. In *Proceedings of the Ninth International Symposium on Computer-Assisted Cartography*, pages 255–265, Baltimore, MD, 1989.

[28] G.J. Hunter, M.F. Goodchild, and M. Robey. A toolbox for assessing uncertainty in spatial databases. In *The Annual Conference of the Australisian Urban and Regional Information Systems Association*, Sydney, New South Wales, 1994.

[29] Swanson F. J. Lienkaemper G.W. and F. Nakamura. Change in landslide hazard through time– a case study of forestry land use and climate change in the Cascade Mountains, Oregon, USA. Unpublished manuscript, 1992.

[30] G.J. Hunter, B. Hock, M. Robey, and M.F. Goodchild. Experimental development of a model of vector data uncertainty. In *Proceedings of the Second International Symposium on Spatial Accuracy Assessment in Natural Resources and Environmental Modeling*, pages 217–224, Fort Collins, CO, 1996.